

On the Nature of Navier-Stokes Turbulence

Robert G. Deissler
Lewis Research Center
Cleveland, Ohio

(NASA-TM-101983) ON THE NATURE OF
NAVIER-STOKES TURBULENCE Ph.D. Thesis - Case
Western Reserve Univ. (NASA Lewis
Research Center) 102 p

N89-23813

CSCL 20D

G3/34 Unclass
0209820

May 1989

NASA

ON THE NATURE OF NAVIER-STOKES TURBULENCE

Robert G. Deissler
National Aeronautics and Space Administration
Lewis Research Center
Cleveland, Ohio 44135

ABSTRACT

Several turbulent and nonturbulent solutions of the Navier-Stokes equations are obtained. The unaveraged equations are used numerically in conjunction with tools and concepts from nonlinear dynamics, including time series, phase portraits, Poincaré sections, largest Liapunov exponents, power spectra, and strange attractors.

Initially neighboring solutions for a low-Reynolds-number fully developed turbulence are compared. The turbulence is sustained by a nonrandom time-independent external force. The solutions, on the average, separate exponentially with time, having a positive Liapunov exponent. Thus the turbulence is characterized as chaotic.

In a search for solutions which contrast with the turbulent ones, the Reynolds number (or strength of the forcing) is reduced. Several qualitatively different flows are noted. These are, respectively, fully chaotic, complex periodic, weakly chaotic, simple periodic, and fixed-point. Of these, we classify only the fully chaotic flows as turbulent. Those flows have both a positive Liapunov exponent and Poincaré sections without pattern. By contrast,

the weakly chaotic flows, although having positive Liapunov exponents, have some pattern in their Poincaré sections. The fixed-point and periodic flows are nonturbulent, since turbulence, as generally understood, is both time-dependent and aperiodic.

By using both the unaveraged Navier-Stokes equations, and the corresponding averaged or moment equations, turbulent solutions are obtained in which energy cascades from large to small-scale motions. In general the spectral energy transfer takes place between wavenumber bands that are considerably separated. The spectral transfer can occur either as a result of nonlinear turbulence self-interaction or by interaction of turbulence with mean gradients. The latter appears to be closely related to a nonuniform or sudden turbulent mixing shown to occur in the presence of mean gradients.

Turbulent systems are compared with those studied in kinetic theory. The two types of systems are fundamentally different (continuous and dissipative as opposed to discrete and conservative), but there are similarities. For instance, both are nonlinear and show sensitive dependence on initial conditions. Also, the turbulent and molecular stress tensors are identical if the macroscopic velocities for the turbulent stress are replaced by molecular velocities.

CONTENTS

	Page
ABSTRACT	i
I. INTRODUCTION	1
II. BASIC EQUATIONS AND A LONG-TERM SOLUTION WITH STEADY FORCING	4
III. SOME TURBULENT AND NONTURBULENT NAVIER-STOKES FLOWS . .	18
A. Time series	20
B. Phase portraits	23
C. Poincaré sections	35
D. Liapunov exponent	41
E. Characterization of the flow for $\chi = 0.338$	49
F. Chaotic versus turbulent flows	49
G. Power spectra	50
H. Dimensions of the attractors	54
IV. TURBULENT ENERGY TRANSFER AND TURBULENT DISSIPATION . .	57
A. Homogeneous turbulence with no mean gradients . . .	63
B. Homogeneous turbulence with a mean shear	76
V. THE SUDDENNESS OF TURBULENT MIXING	85
VI. CONCLUSION	91
REFERENCES	95

I. INTRODUCTION

Fluid turbulence is a many-faceted phenomenon. It has been characterized as random, nonlinear, multiscaled, dissipative, as having a negative velocity-derivative skewness factor, as transferring energy (mainly) to small-scale motions, as being dissipated by small-scale motions, as tending toward isotropy, and as having an infinite number of components or degrees of freedom. Those descriptions appear in what might now be called the classical or statistical theory of turbulence.¹⁻⁴ That theory is based mainly on averaged or moment equations obtained from the Navier-Stokes equations.

The idea of using averaged equations, rather than the unaveraged Navier-Stokes equations directly in an analysis, has been adopted in the past mainly because it was thought that averaged, smoothly varying quantities should be easier to deal with than the haphazard motions occurring in the unaveraged equations. However because of the nonlinearity of the Navier-Stokes equations, the averaging process introduces the closure problem (more unknowns than equations),¹ so that it is not clear that averaging is advantageous as far as getting solutions is concerned. The averaged or moment equations are, however, useful for discussing the physical processes occurring in turbulence.⁴

In recent years there have been attempts to utilize concepts from the theory of nonlinear dynamical systems in the analysis of turbulence.⁵⁻⁹ There, in contrast to the statistical theory, the emphasis is on unaveraged, rather than on averaged equations. The use of unaveraged equations in which the velocities vary in a complicated way is made feasible by the advent of high speed computers. By using ideas from nonlinear dynamics one might (as further evidence that turbulence is a many-faceted phenomenon) characterize turbulence as chaotic, as aperiodic, as having sensitive dependence on initial conditions, as having time series without pattern, as having a positive Liapunov exponent, as having a phase portrait without pattern, as having Poincaré sections without pattern, as lying on a strange or chaotic attractor, and as having continuous time and spatial spectra.

Both the statistical (classical) theory and the newer nonlinear dynamics theory provide valid ways of looking at turbulence. The latter furnishes a number of new tools for probing the nature of turbulence (e.g., Liapunov exponents, Poincaré sections, etc.). But as yet it does not seem to provide a means of discussing such well-known aspects of turbulence as spectral and directional transfer of energy. Those aspects can, however, be considered within the framework of conventional turbulence theory.

Here we study the nature of Navier-Stokes turbulence; that is, we consider the turbulence obtained in solutions of the Navier-Stokes equations. In order to obtain as clear a picture as possible, use is made of concepts both from nonlinear dynamics and from the more conventional (statistical) turbulence theory. Sensitive dependence on initial conditions, strange attractors, and spectral transfer between wavenumbers are included. All of those are shown to occur in turbulence by obtaining and interpreting (mainly numerical) solutions of the Navier-Stokes equations.

In order to give a sharper characterization of turbulence, turbulent solutions are contrasted with periodic, quasiperiodic, and fixed-point solutions. Turbulent systems are also compared with those considered in the kinetic theory of gases. It is shown that there is a certain suddenness inherent in turbulent mixing, as there is in molecular mixing by collision of gas particles.

II. BASIC EQUATIONS AND A LONG-TERM TURBULENT SOLUTION WITH STEADY FORCING

The incompressible Navier-Stokes equations, on which the present study is based, are

$$\frac{\partial u_i}{\partial t} = - \frac{\partial(u_i u_k)}{\partial x_k} - \frac{1}{\rho} \frac{\partial p}{\partial x_i} + \nu \frac{\partial^2 u_i}{\partial x_k \partial x_k} + F_i, \quad (1)$$

together with a Poisson equation for the pressure

$$\frac{1}{\rho} \frac{\partial^2 p}{\partial x_\ell \partial x_\ell} = - \frac{\partial^2(u_\ell u_k)}{\partial x_\ell \partial x_k} + \frac{\partial F_\ell}{\partial x_\ell}. \quad (2)$$

The subscripts can have the values 1, 2, or 3, and a repeated subscript in a term indicates a summation, with the subscript successively taking on the values 1, 2, and 3. The quantity u_i is an instantaneous velocity component, x_i is a space coordinate, t is the time, ρ is the density, ν is the kinematic viscosity, p is the instantaneous pressure, and F_i is a time-independent forcing term, or external force, which is taken as some fraction χ of the negative of the initial viscous term at $t = 0$. That is,

$$F_i = -\chi \nu \left(\frac{\partial^2 u_i}{\partial x_k \partial x_k} \right)_{t=0}. \quad (3)$$

The fraction χ controls the value of the asymptotic Reynolds number of the flow. The initial nonrandom u_i in Eq. (3) are given at $t = 0$ by^{7,8}

$$u_j = a_j \cos q \cdot x + b_j \cos r \cdot x + c_j \cos s \cdot x, \quad (4)$$

where

$$\begin{aligned} a_j &= k(2,1,1), & b_j &= k(1,2,1), & c_j &= k(1,1,2), \\ q_j &= (-1,1,1)/x_0, & r_j &= (1,-1,1)/x_0, & s_j &= (1,1,-1)/x_0, \end{aligned} \quad (5)$$

k is a quantity that fixes the initial Reynolds number at $t = 0$, and x_0 is one over the magnitude of an initial wavenumber component. Through Eq. (3), x_0 is also one over the magnitude of a wavenumber component of the forcing term F_j . Equations (4) and (5) satisfy continuity, and Eqs. (1) to (3) insure that continuity is maintained. Moreover Eqs. (3) to (5) give local values of F_j which are symmetric with respect to 90° rotations and translations of $2\pi x_0$. Then we find numerically that

$$\overline{u_1^2} \approx \overline{u_2^2} \approx \overline{u_3^2} \quad (6a)$$

at all times, where the overbars indicate values averaged over space. After the initial transients have died out, the averages may also be taken over time, and the inexact equalities in Eq. (6a) become equalities. Equation (6a) then becomes

$$\overline{\overline{u_1^2}} = \overline{\overline{u_2^2}} = \overline{\overline{u_3^2}}, \quad (6b)$$

where the double bars indicate averages over space and time. The boundary conditions are periodic with a period of $2\pi x_0$. From Eq. (3) and continuity, the last term in Eq. (2) is zero for our system.

Equation (1) is a nonlinear dissipative equation for the evolution of the vector u_i . Although a Navier-Stokes fluid is linear (stress proportional to strain rate), a nonlinearity appears in Eq. (1) as an effect of inertia. The equation is autonomous, since time does not appear explicitly on the right side, and deterministic since there are no random coefficients. Note that the equation would not be autonomous if the forcing term F_i were time-dependent. Equation (1), although three-dimensional in physical space, is infinite-dimensional in phase (or state) space, since it is a partial differential equation. (The number of dimensions of the phase space of our system is the number of u_i 's required to specify the velocity field at a particular time. The pressure is not specified; it is calculated from Eq. (2).) The equation can be converted to an infinite system of ordinary differential equations by, for instance, introducing finite-difference representations of spatial derivatives (and letting grid spacing approach 0), or by taking the spatial Fourier transform of the equation. Because it is dissipative, the infinite system can be represented by a finite system of equations.¹⁰ There should be a viscous cutoff, below which motion becomes unimportant as the scale of the motion decreases. Thus a numerical solution should be possible, at least for low Reynolds numbers. Equation (1), together with Eq. (2) for the pressure, Eqs. (3) to (5) for the forcing term, Eqs. (4) and (5) for the initial conditions, and periodic boundary conditions,

can be considered a nonlinear, deterministic, autonomous, dissipative, dynamical system. The system is deterministic, since there are no random elements in Eqs. (1) to (5) or in the boundary conditions.

The numerical method used for the solution of Eqs. (1) to (5) has been given previously.^{7,11} A cubical computational grid (32^3 grid points), fourth-order spatial differencing, and third-order predictor-corrector time differencing are used. In order to obtain numerical stability for the highest asymptotic Reynolds number (13.3), it was necessary to use about 50 time steps in each small fluctuation of velocity, so that the fluctuations with respect to time are well resolved indeed. The spatial resolution is also good and will be discussed later, in connection with Fig. 5.

It follows from Eqs. (3) to (5) that the nonrandom initial condition on u_i applied at $t = 0$ is proportional to the steady forcing term F_i . The quantity $(u_i)_{t=0}$, or F_i , on an $x_j - x_k$ plane through the numerical grid center is plotted in Fig. 1. Figure 2 shows the magnitude of the vector $(u_i)_{t=0}$ or F_i . A high degree of spatial symmetry of $(u_i)_{t=0}$ and of F_i is apparent from these plots. Note that as a result of the symmetry, the subscript i can designate any component of the vectors, and that the $x_j - x_k$ plane can be any plane through the numerical grid center parallel to the grid axes. That is, i, j , and $k = 1, 2$, or 3 ; $j \neq k$. Moreover, the symmetry allows the development of symmetric turbulence in a box, where the box has periodic walls.

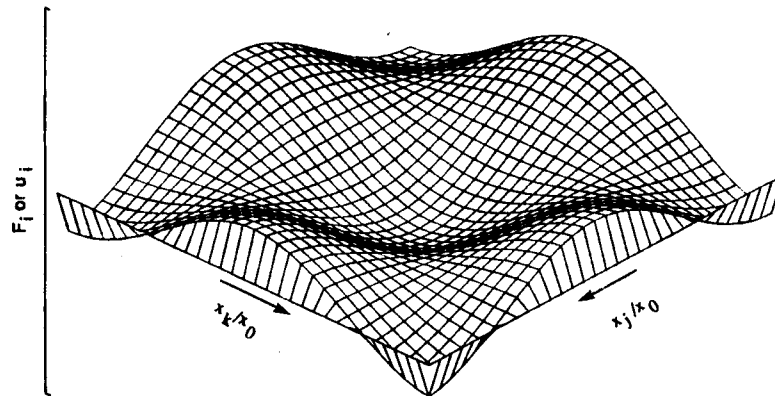


Figure 1. - Plot of forcing term F_i in Eq. (1) or of regular initial velocity component u_i on a plane through center of numerical grid. x_k and x_j are coordinates on the plane and x_0 is the reciprocal of a wave-number component of the forcing term.

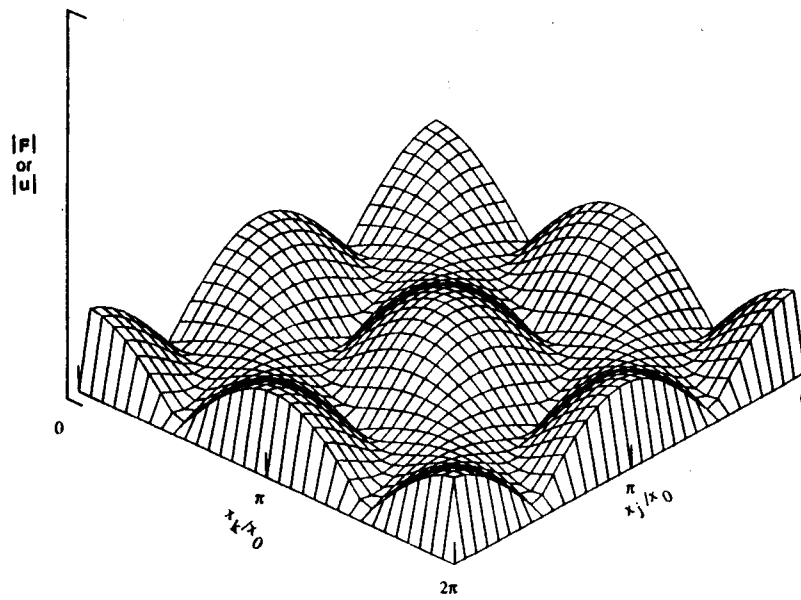


Figure 2. - Magnitude of forcing vector or of regular initial velocity vector on a plane through numerical-grid center.

Results for the evolution of $(\overline{u_1^2})^{1/2}$ for x in Eq. (3) equal to 1 (asymptotic Reynolds number, 13.3) are given in Fig. 3 (see Fig. 3 for definition of the Reynolds number). The value of k in Eq. (5) is 20, giving an initial Reynolds number at $t = 0$ of 34.6. The velocities have been divided by $(\overline{u_0^2})^{1/2}$, where the 0 again refers to $t = 0$. An asymptotic turbulent solution is obtained for $t^* > 5$. (The asterisk on t indicates that it has been nondimensionalized by x_0 and v .)

A rather remarkable feature of turbulent flow is that a time-dependent haphazard flow can result when the applied exciting forces are steady (e.g., in a fully developed turbulent pipe flow with a steady applied pressure gradient). Figure 3 shows that the Navier-Stokes turbulence calculated here exhibits this feature, since a steady forcing term produces an apparently haphazard time-dependent motion. This is evidently an indication of the inherent instability of the nonlinear Navier-Stokes equations except at very low Reynolds numbers. It will later be seen that our steady forcing term can also produce time-dependent *nonturbulent* flow.

It should be mentioned that the symmetry present in the initial conditions (Eqs. (4) and (5)) which, for instance, causes the three local velocity components to be equal for $x_1 = x_2 = x_3$ at $t = 0$, has been destroyed before $t^* = 5$, apparently by roundoff errors. This symmetry breaking for local values must indeed occur in order for true turbulence to develop, and in fact the fluctuations eventually die out if the symmetry remains. Here

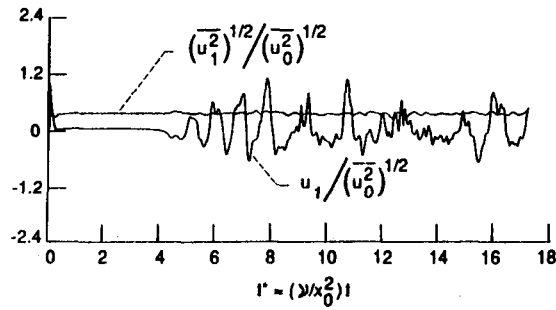


Figure 3. - Calculated evolution of turbulent velocity fluctuations with a time-independent forcing term. Ordinates normalized by initial condition. Root-mean square velocities (with a single bar) are spatially averaged. Developed Reynolds number $(\overline{u_1^2})^{1/2} x_0 / \nu = 13.3$, where the double bar indicates an average over space and time for $t^* > 5$, $x = 1$. $x_1^* = x_1 / x_0 = 9\pi/8$, $x_2^* = 21\pi/16$, $x_3^* = 23\pi/16$, for unaveraged fluctuations. 32^3 spatial grid points.

the initial fluctuations were not strong enough to destroy the symmetry before the fluctuations become too small to be seen on the u_1 curve. The symmetry breaking apparently occurred on the flat portion of the curve by the accumulation of roundoff errors. For higher initial Reynolds numbers (not shown) the initial fluctuations were strong enough to break the local symmetry earlier, and the flat portion of the u_1 curve was absent.

The mean skewness factor S of the velocity derivative of our Navier-Stokes turbulence in Fig. 3 is calculated to be

$$S = \frac{\overline{\left(\frac{\partial u_1}{\partial x_1}\right)^3}}{\left[\overline{\left(\frac{\partial u_1}{\partial x_1}\right)^2}\right]^{3/2}} = -0.52, \quad (7)$$

where the skewness factor is averaged over time after the powers of the velocity derivative have been averaged over space. This value is close to those obtained experimentally for a variety of simple turbulent flows,¹² where the Reynolds numbers of the experiments were in the same range as that for the solution in Fig. 3.

Instantaneous (unaveraged) terms in the Navier-Stokes equation (Eq. (1)) for $i = 1$ at the numerical grid center are plotted in Fig. 4. These include the nonlinear convective term $-\partial(u_j u_k)/\partial x_k$, the steady forcing term F_i , the viscous term $\nu \partial^2 u / \partial x_k \partial x_k$, and the pressure term $-(1/\rho) \partial p / \partial x_i$.

For the asymptotic or developed region (for $t^* > 5$) the viscous term is of the same order of magnitude as the steady

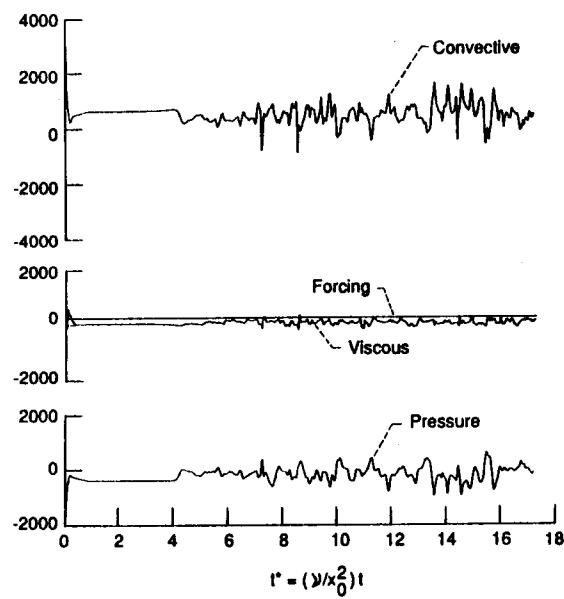


Figure 4. - Calculated evolution of instantaneous terms in Navier-Stokes equation at grid center. $\chi = 1$. Developed Reynolds number = 13.3.

forcing term. This is reasonable since the forcing term replenishes the energy lost by viscous action. On the other hand the nonlinear convective and pressure terms are much larger. (The pressure term is nonlinear through Eq (2).) It may seem surprising that a small forcing term can produce large convective and pressure terms; apparently those terms are amplified by the instability of the Navier-Stokes flow at the Reynolds number in Fig. 3. The tendency is even greater at higher Reynolds numbers (not shown). If we compare the nonlinear convective and pressure terms with the viscous term rather than with the forcing term, the trend is not surprising, since it is well-known that the nonlinear terms become much greater than the viscous as the Reynolds number of a turbulent flow increases. As was mentioned before, the forcing term is of the same order of magnitude as the viscous.

Calculated spatial variations of velocity fluctuations are plotted in Fig. 5. Although the Reynolds number is low, there is some tendency for velocity gradients to become large in some regions, thus indicating the hydrodynamic instability of the flow. This tendency to form steep gradients is, of course, a well-known property of turbulent flows. In order to give an idea of the numerical resolution obtained, grid points are indicated by symbols; all of the scales of motion are well resolved.

The number of degrees of freedom or modes used in the present solution (32^3 grid points times three directional velocity components) was compared with the criteria for sufficient

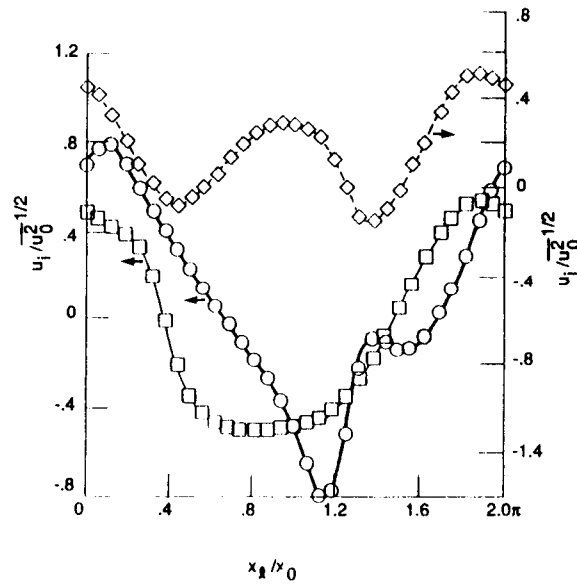


Figure 5. - Calculated spatial variation of velocity fluctuations on a plane through grid center at $t^* = 13.74$. Symbols are at grid points. -O- $i = 2, l = 1$; -□- $i = 2, l = 2$; -◇- $i = 1, l = 1$.

determining modes obtained by Constantin et al.¹⁰ Both on the basis of the ratio of the largest to smallest length scale and on the basis of Reynolds number, the number of determining modes used in the present solution was considerably larger than required for a qualitatively correct solution. So according to the criteria of reference 10, there are plenty of determining modes for a qualitatively correct solution. That reference does not address the problem of a quantitatively correct solution.

After initial transients have died out (for $t^* > 5$), the flow considered in Figs. 1 to 7 lies on a strange attractor. This is because, as shown,⁸ the flow exhibits sensitive dependence on initial conditions, and because the Navier-Stokes equations represent a dissipative system, so that volumes in phase space, on the average, contract (for large times volumes in phase space approach zero!).^{6,7,13} We have also shown that sensitive dependence on initial conditions occurs for decaying turbulence.⁷

Figure 6 shows an instantaneous velocity vector field in the asymptotic (developed) region projected on the $x_1 - x_2$ plane through the numerical grid center. The time is $t^* = 13.28$. A few instantaneous streamlines have also been sketched in. The flow in Fig. 6 appears to be composed of random jets and whirls; other projections of the velocity vector field have a similar appearance, but with jets and whirls at different locations.

A three-dimensional representation of an instantaneous velocity field in the asymptotic region is given in Fig. 7. The

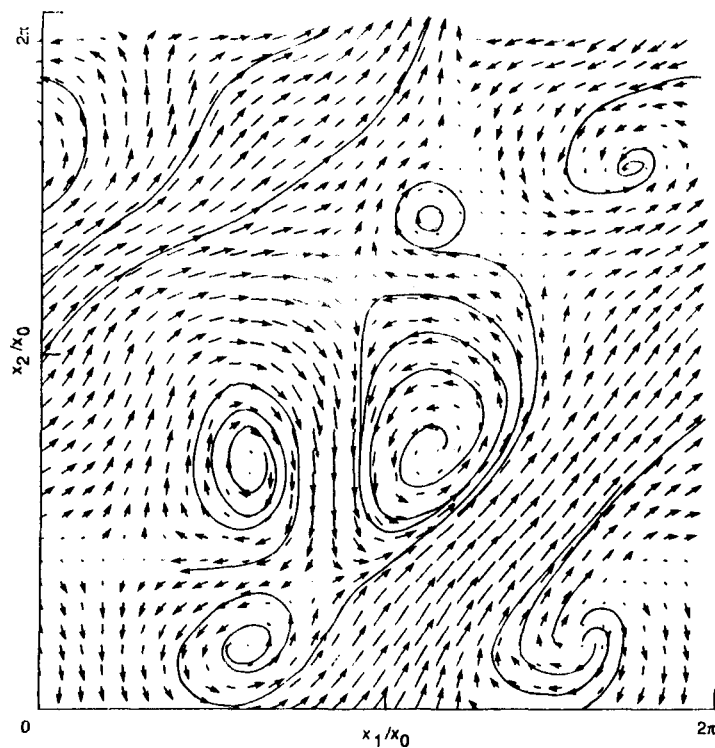


Figure 6. - Plot of projection of velocity-vector field on $x_1 - x_2$ plane through grid center. Lengths of arrows are proportional to velocity magnitudes. Also shown are some streamlines. $x = 1$. $t^* = 13.28$.

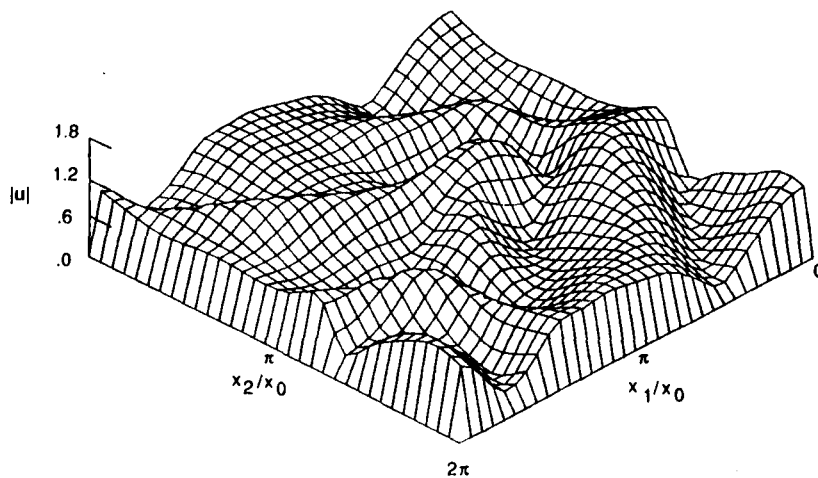


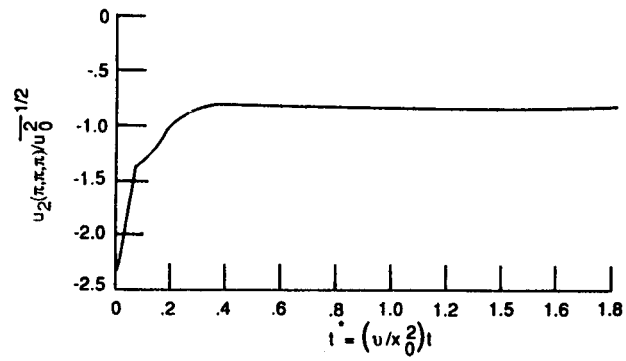
Figure 7. - Magnitude of spatially chaotic initial velocity vector on plane through grid center. $t^* = 13.28$

magnitude of the velocity vector $|\mathbf{u}|$ is plotted on the $x_1 - x_2$ plane through the numerical grid center. The time is again $t^* = 13.28$. Figure 7, as well as Fig. 6, illustrates the chaotic appearance of the velocity field. It is evident that the symmetry present in the nonrandom initial conditions in Figs. 1 and 2 has been broken for the developed flow in Figs. 6 and 7.

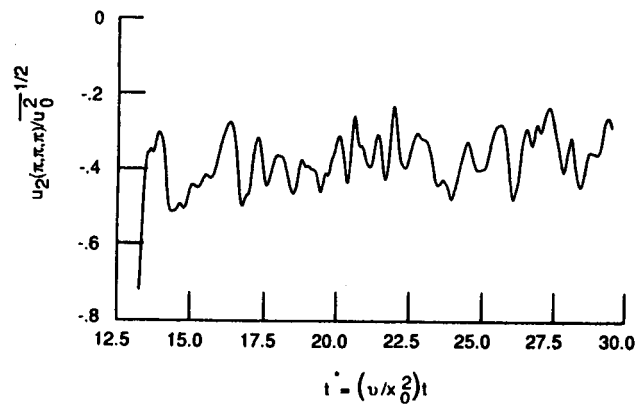
III. SOME TURBULENT AND NONTURBULENT NAVIER-STOKES FLOWS

In this section (except for one of the flows considered for illustrative purposes in Fig. 8) we will use as initial conditions the spatially chaotic conditions in Figs. 6 and 7. These correspond to the flow in Fig. 3 at $t^* = 13.28$. As shown,⁸ that flow is chaotic (the Liapunov characteristic exponent is positive). The use of chaotic initial conditions tends to assure that the unstable modes in a given flow are excited.

The effectiveness of chaotic initial conditions in exciting unstable modes is illustrated in Fig. 8. The Reynolds numbers of both the *nonchaotic* initial conditions and of the asymptotic flow in Fig. 8(a) are higher than those in Fig. 8(b), where the initial conditions are *chaotic*. Since the asymptotic flow in Fig. 8(a) is time-independent and that in Fig. 8(b) is chaotic, one sees that the character of these asymptotic flows is controlled by whether or not the initial conditions are chaotic, rather than by the Reynolds numbers. Of course if the initial Reynolds number is high enough, as in Fig. 3, the asymptotic flow may be chaotic even if the initial conditions are regular. At any rate it is clear from Fig. 8 that the use of chaotic initial conditions tends to make the asymptotic flow chaotic, when that is possible. It tends to insure that unstable modes are excited. But it will be seen that, depending on the final Reynolds number, a variety of asymptotic flows can be obtained from chaotic initial conditions.



(a) Initial flow, regular. Initial Reynolds number = 17.3.
Asymptotic Reynolds number = 8.5.



(b) Initial flow, chaotic. Initial Reynolds number = 13.3.
Asymptotic Reynolds number = 7.4.

Figure 8. - Effects of type of initial flow and of Reynolds number on asymptotic flow.

The procedure for the calculations in the remainder of this section is this: The initial conditions, which are spatially chaotic, are obtained from the chaotic flow in Fig. 3 for $t^* = 13.28$. (See also Figs. 6 and 7.) Using that initial condition, the asymptotic Reynolds number for each flow is fixed by setting the value of χ in the forcing term in Eq. (3).

A. Time series

Time series for six different low-Reynolds-number flows are shown in Figs. 9 and 3. In Fig. 9(a), where the asymptotic Reynolds number Re_a is 4.78 ($\chi = 0.2$), the asymptotic (long-time) flow is time-independent. This happens although the initial conditions are chaotic. Thus the Reynolds number here appears not to be high enough to sustain a time-dependent chaotic or periodic flow; no modes are active. In phase space this type of flow is a fixed point, as will be discussed in the next section.

For an asymptotic Reynolds number of 6.24 ($\chi = 0.3$) the long-term solution shown in Fig. 9(b) is periodic in time. The curve has a rather simple shape, although it is not as simple as a sine wave. As discussed in the next section, this is a limit cycle in phase space.

The asymptotic flow in Fig. 9(c), which is for a Reynolds number of 6.72 ($\chi = 0.338$), has some parts which appear to repeat, but it is not periodic. Even after a very long time we were unable to obtain a complete repeating cycle. In order to see if roundoff errors could produce that result, we increased those errors by

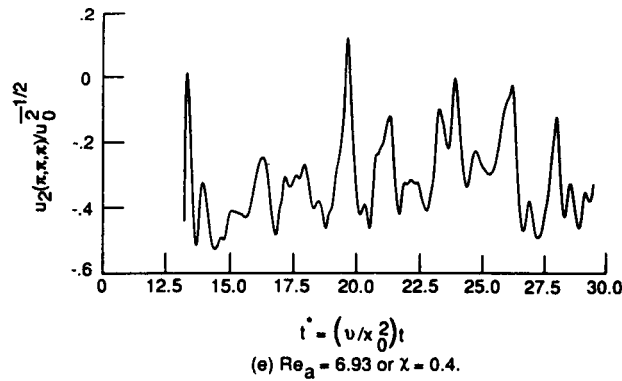
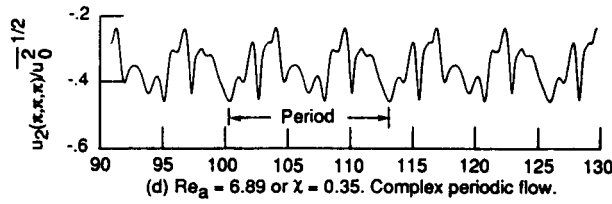
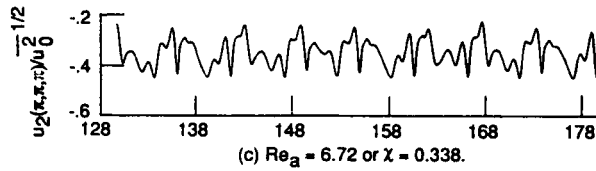
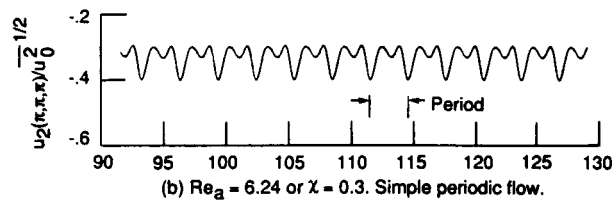
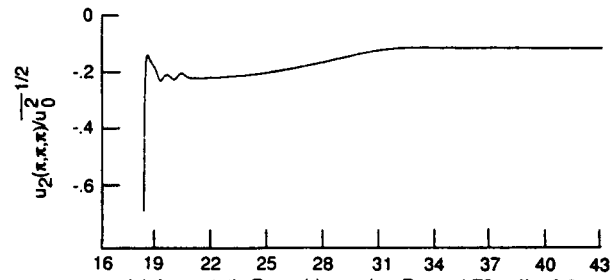


Figure 9. - Calculated time series for evolution of velocity component. Initial flow, chaotic. Initial Reynolds number = 13.3.

several orders of magnitude, but the results were unchanged. Figure 9(c) by itself does not provide enough information to characterize the flow in that figure. After we have calculated phase portraits, Poincaré sections, and Liapunov exponents, we will be in a better position to characterize the flow.

Consider next the asymptotic flow in Fig. 9(d), where the Reynolds number is 6.89 ($\chi = 0.35$). At first glance this flow might appear chaotic because of its complexity. It is, however, periodic, although the velocity variation within each period is quite complicated. This complex periodic flow has a period close to four times that of the simple periodic flow in Fig. 9(b). We discovered these two flows (periods 1 and 4) before the nonperiodic one in Fig. 9(c). It was thought that it would be easy to find a period 2 flow by using a value of χ between 0.3 and 0.35, and thus to demonstrate period-doubling. However the cases we tried ($\chi = 0.338$ and 0.341), starting either from chaotic initial conditions or from the period 4 flow in Fig. 9(d), gave nonperiodic flows similar to that in Fig. 9(c). Thus our route to turbulence turned out to be more complicated than anticipated.

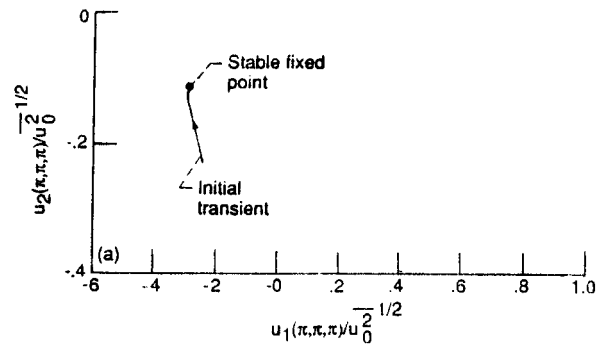
Finally, by increasing the asymptotic Reynolds number to 6.93 ($\chi = 0.4$) we get in Fig. 9(e) what appears to be a chaotic flow, since it has no apparent pattern. The flow has an appearance similar to that in Fig. 3 ($\chi = 1$) which was already shown to be chaotic.⁸

In summarizing the information obtained from the time series for the various asymptotic flows, we note that the only flows that could be identified with reasonable certainty from the time series alone were the time-independent flow (Fig. 9(a)) and the periodic flows in Figs. 9(b) and (d). We will be able to get a better understanding even of those flows from representations yet to be considered.

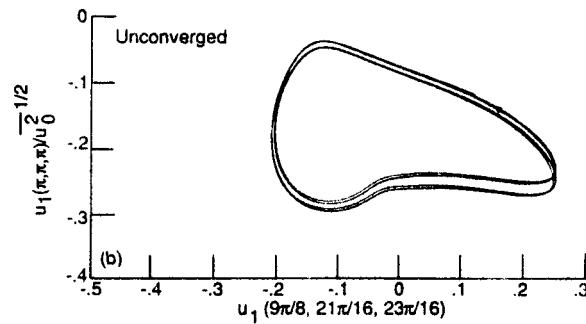
B. Phase portraits

The term "phase portrait" as used here refers to a solution trajectory in the phase space of a flow. Since one cannot readily visualize a space of more than three dimensions, our representations will be projections of the higher-dimensional portraits onto two-dimensional planes or three-dimensional volumes in phase space.

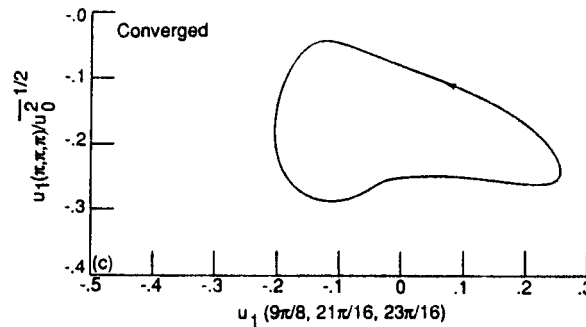
The trajectory in Fig. 10(a), which corresponds to the time series in Fig. 9(a), shows an initial transient which ends at a stable fixed point in phase space. The arrow indicates the direction of increasing time (the direction of motion of the phase point). Since the velocity components at all points in physical space are time independent for large times, the phase point occupies the same position in phase space for all large times. The projection in Fig. 10(a) is onto a $u_1(\pi, \pi, \pi) - u_2(\pi, \pi, \pi)$ plane; other projections are similar. This is the simplest example of an attractor, the trajectory in phase space being attracted to a single stable point. Once the phase point arrives



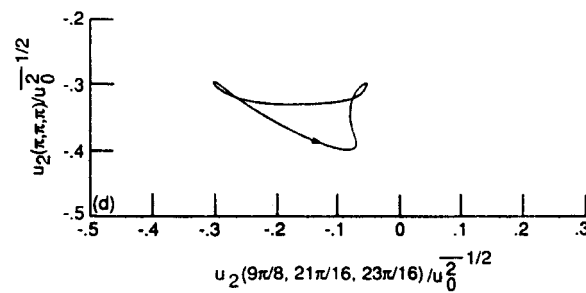
$Re_a = 4.78$ or $\chi = 0.2$. Transient and fixed point flow. $t^* > 21$.



$Re_a = 6.24$ or $\chi = 0.3$. Simple periodic flow.

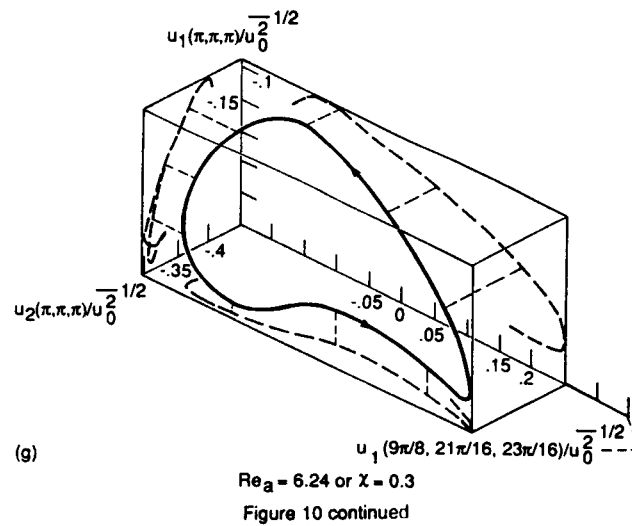
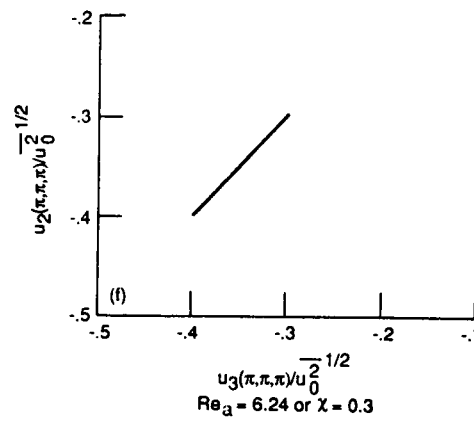
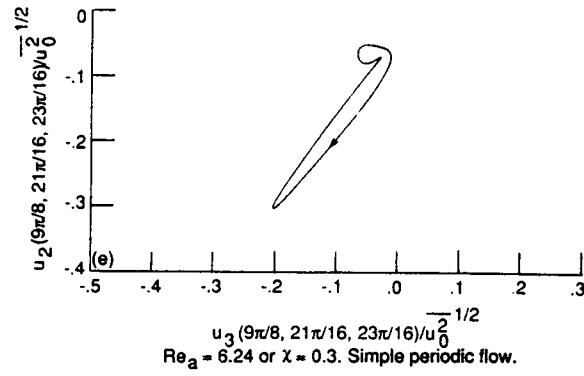


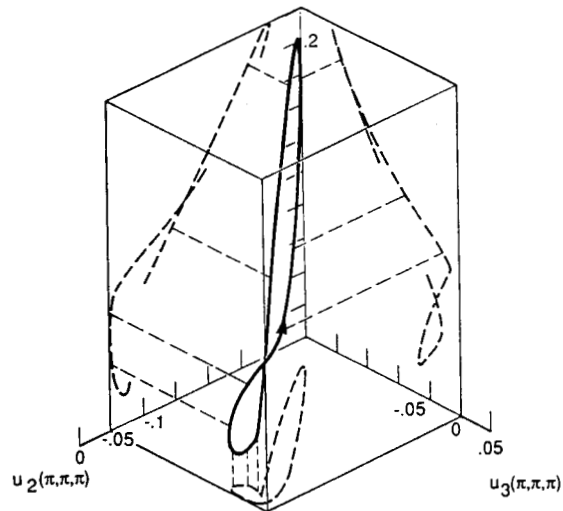
$Re_a = 6.24$ or $\chi = 0.3$.



$Re_a = 6.24$ or $\chi = 0.3$.

Figure 10. - Projected phase portraits.





(h)

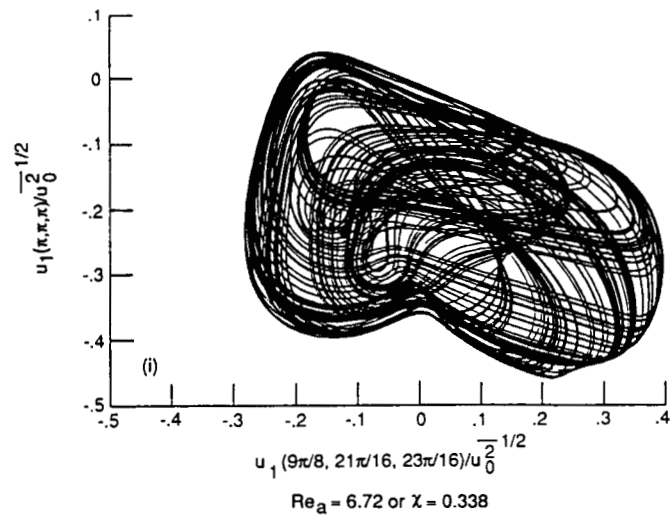
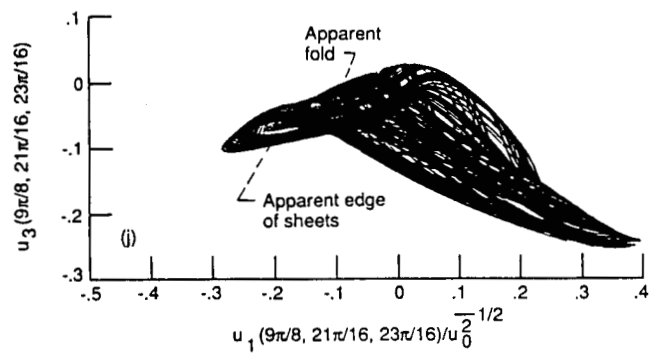
 $Re_a = 6.24$ or $\chi = 0.3$. Simple periodic flow. $Re_a = 6.72$ or $\chi = 0.338$  $Re_a = 6.72$ or $\chi = 0.338$

Figure 10 continued.

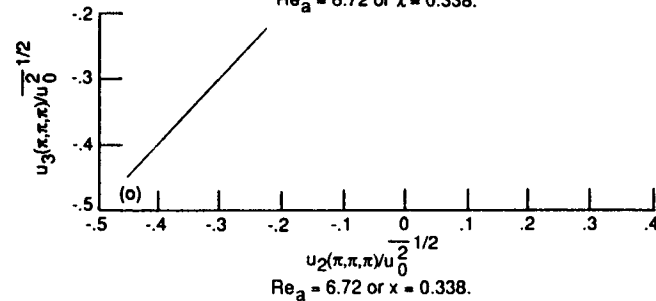
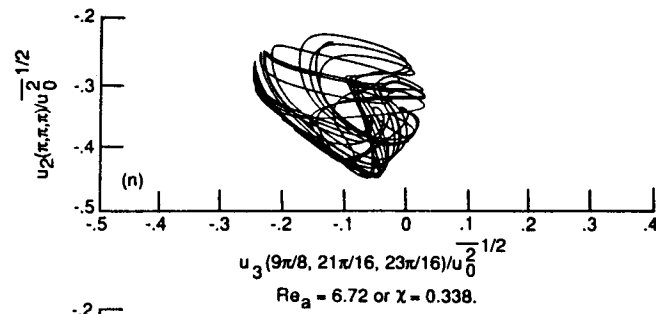
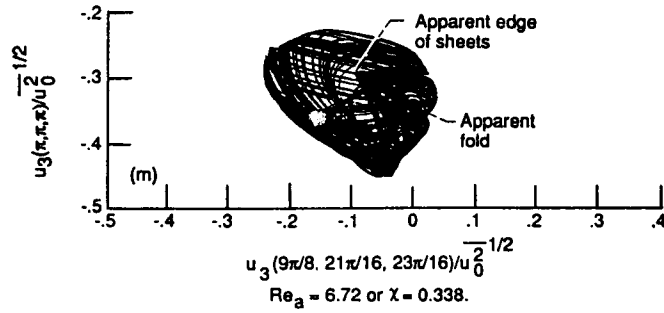
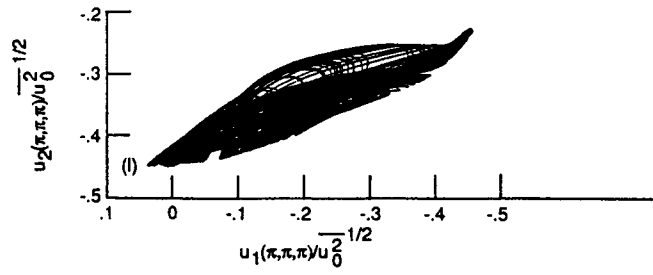
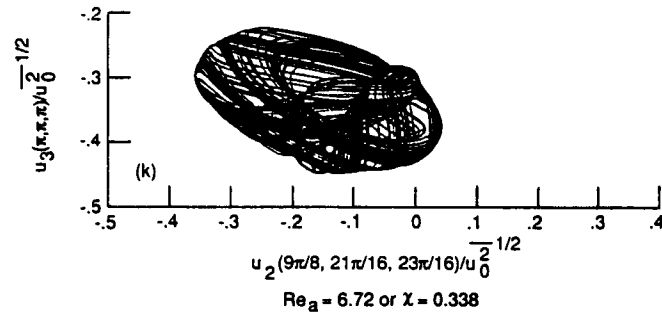


Figure 10 continued.

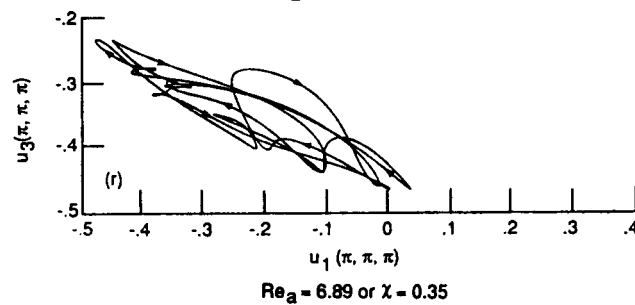
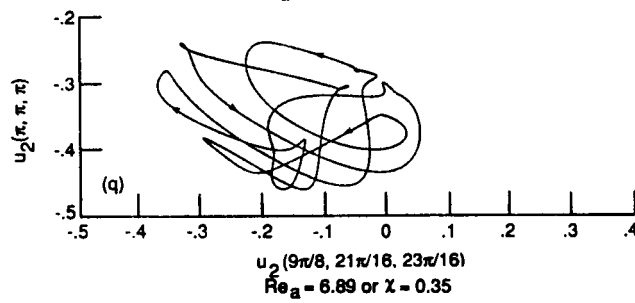
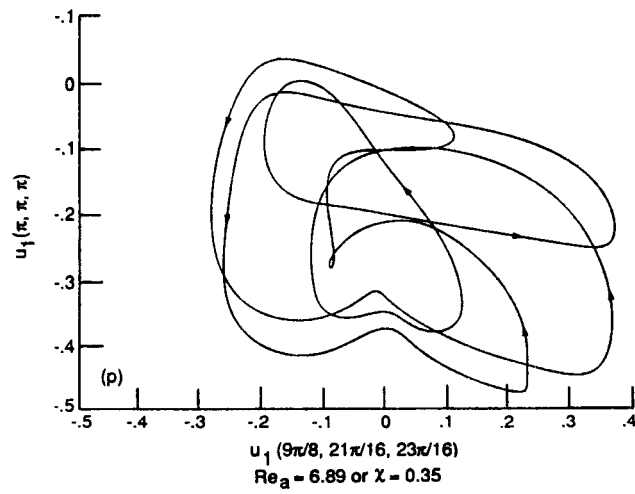


Figure 10 continued.

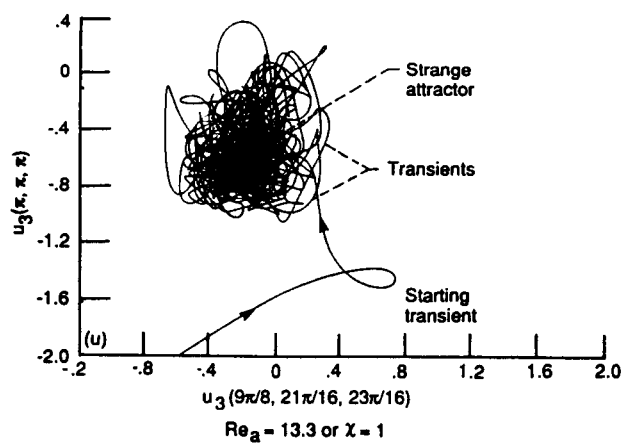
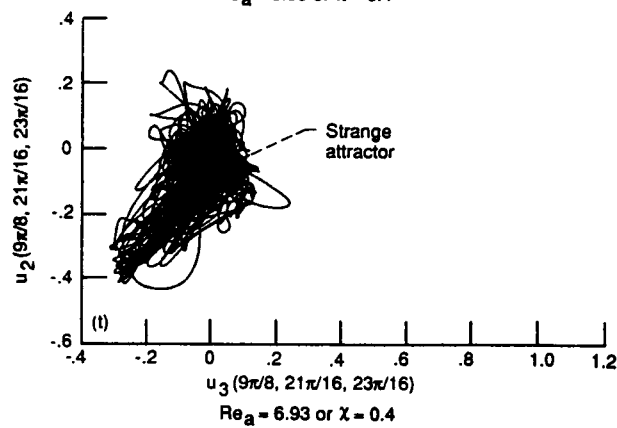
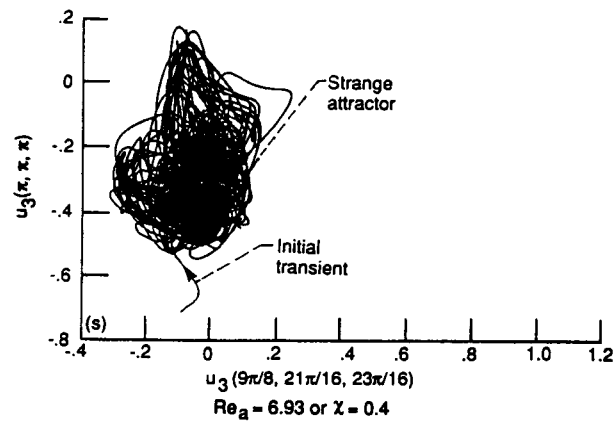


Figure 10 continued.

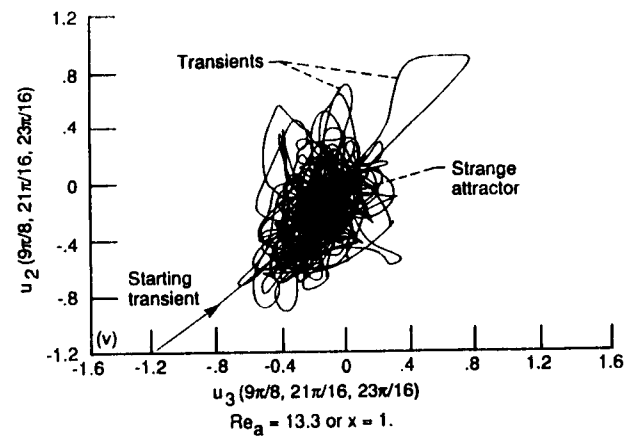


Figure 10 concluded.

there it does not leave. As mentioned earlier, volumes in phase space contract, on the average, in a dissipative system.¹³ In this case the volumes shrink down to a zero-volume zero-dimensional point. Motion in physical space does not of course cease but becomes time-independent.

Consider next the periodic phase portrait corresponding to the time series in Fig. 9(b) (see Figs. 10(b) to (h)). Figures 10(b) and (c) show trajectories projected onto a u_1 ($9\pi/8$, $21\pi/16$, $23\pi/16$) - $u_1(\pi, \pi, \pi)$ plane. Comparison of the unconverged orbit in Fig. 10(b) with the converged one in Fig. 10(c) shows that the unconverged curve wobbles around (on both sides of) the converged curve until it finally settles down on the latter. Thus the trajectory is attracted to a stable limit cycle or periodic attractor. The fact that the phase point traces the same curve over and over (after convergence) confirms the periodicity of the orbit.

The contraction of volumes in phase space for a dissipative system again manifests itself here. Whereas in Fig. 10(a) the volumes shrink down to a zero-volume zero-dimensional point, for the periodic attractor considered here they shrink down to a zero-volume *one*-dimensional closed line. The coordinate axis used to plot the line will have the same shape as the line. Thus although the line itself is one-dimensional, the one-dimensional coordinate system, or the basis function, may require many orthogonal dimensions to represent it. The line is, strictly

speaking, one-dimensional only when used with its own optimum one-dimensional coordinate system or basis function. Although the line will not cross itself in its optimum coordinate system, it may cross when projected onto a two-dimensional orthogonal coordinate system (see Fig. 10(d)).

Additional projections of the periodic attractor onto planes in phase space are shown in Figs. 10(e) and (f) in order to give an idea of the variety of curve shapes that can be obtained. Note that in Fig. 10(f), part of the symmetry present for $t = 0$ (Fig. 1) has returned. (This symmetry is absent in the fully chaotic flows.) Projections of the orbit onto three-dimensional volumes in phase space are plotted in Figs. 10(g) and (h).

Phase-portrait projections corresponding to the time series in Fig. 9(c) are plotted in Figs. 10(i) to (o). This portrait differs qualitatively from the others shown so far, since it tends to fill a region of space in most of the two-dimensional projections. It was found that the longer the running time, the blacker is the portrait for the projections in Figs. 10(i) to (n). Thus the trajectory is clearly not periodic, since if it were, it would be a closed line in all projections. If it were quasiperiodic (with two independent frequencies), the phase portrait would lie on a torus. Figure 10(k) resembles a torus in some respects, but is more complicated. In particular, it has a knob in the central region.

The projections in Figs. 10(j), (l), and (m) appear to show a sheet-like structure. Whereas for the periodic attractor of Figs. 10(c) to (h), phase-space volumes shrink down to a zero-volume line, here they appear to shrink down to a zero-volume sheet (or sheets). The notch in the projection in Fig. 10(l) is probably the result of a superposition of sheets. Sheet-like structures with folds are generic in strange attractors.⁶ Since in a chaotic flow there is stretching in at least one direction in phase space, there must be folding in order to keep the flow bounded. There appear to be some folds in the projections in Figs. 10(j), (k), and (m), thus indicating that chaos is probable. The confused appearance of the trajectories in Figs. 10(i) and (n) is also indicative of chaos. Further evidence relative to the classification of this hard-to-classify flow will be considered in succeeding sections.

Projections of the periodic trajectory corresponding to the time series in Fig. 9(d) are plotted in Figs. 10(p) to (r). Initial transients have died out. Because of the very complicated appearance of the trajectory a cursory look might lead one to guess that it is chaotic (see also Fig. 9(d)). It is not chaotic, however, since it is not space filling. No matter how long a time the solution is continued, there is no blackening of the phase portrait; the same closed curve is traced over and over, indicating periodicity of the orbit. Since initial deviations or transients present in the flow (not shown) die out as the flow is attracted

to a limiting line, the long-term solution trajectory is a periodic attractor or limit cycle. The flow appears to have a remarkable memory in being able to repeat such a complicated orbit. The fact that such a complicated curve can be retraced is also indicative of the accuracy of the numerical method. As was the case for the simple periodic attractor considered earlier, the present periodic attractor, although much more complicated, shows the shrinking of phase-space volumes to a zero volume one-dimensional line. The discussion given there concerning the sense in which the line is one-dimensional also applies here.

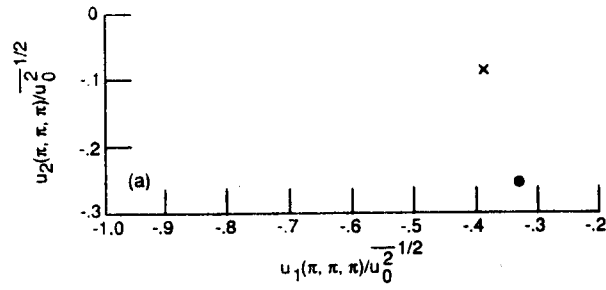
Increasing the Reynolds numbers to those in Figs. 9(e) and 3 we again get (as for Figs. 10(i) to (m)) space-filling attractors. Projections of these are plotted in Figs. 10(s) to (v). After transients have died out, the trajectories are attracted to the black regions in the plots. These look like astrophysical black holes. Indeed, these attractors are similar to black holes in that for large times the phase points cannot leave. A possible difference is that for somewhat earlier times, the phase points can cross over the attractors, leaving them momentarily. However that situation is temporary. After initial transients have completely died out, the phase points must remain forever on the attractors. These trajectories appear to be even more chaotic (have less of a pattern) than those in Figs. 10(i) to (m). However sheets and folding are less apparent than in the attractors for the lower Reynolds number in Figs. 10(i) to (m), probably

because of the higher dimensionality of the attractors for the higher Reynolds numbers. More will be said about that in section H.

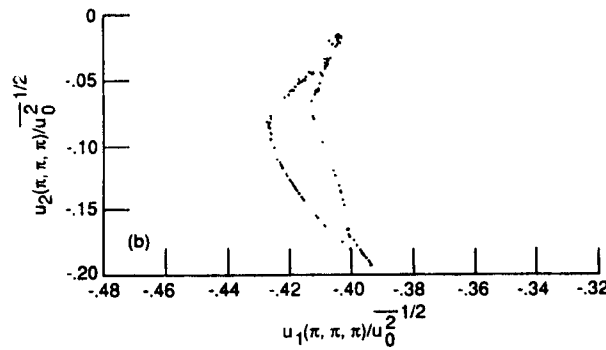
C. Poincaré sections

Poincaré sections are obtained by plotting the points where the phase point of a trajectory pierces (with increasing time) one side of a plane in phase space. The resulting plot has a dimension one less than that of the corresponding phase portrait. The lower-dimensional Poincaré section is sometimes easier to interpret. Here the pierced plane (Poincaré plane) is taken as a $u_1(\pi, \pi, \pi) - u_2(\pi, \pi, \pi)$ plane, and points are plotted when $u_1(9\pi/8, 21\pi/16, 23\pi/16)$ changes from positive to negative or from negative to positive. (Fig. 10(g) may aid in visualizing the operation, at least for the simple periodic case).

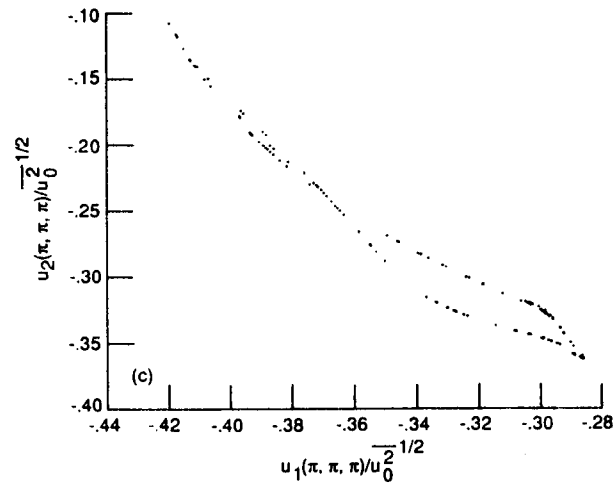
For the fixed-point attractor in Fig. 10(a) a Poincaré section does not exist, since the phase point does not pass through a plane as time increases. So we go on to the simple periodic attractor of Figs. 10(b) to (h). For that attractor the Poincaré sections are points. Figure 11(a) shows two Poincaré sections, one for $u_1(9\pi/8, 21\pi/16, 23\pi/16)$ changing from positive to negative and one for that coordinate changing from negative to positive as the phase point passes through a $u_1(\pi, \pi, \pi) - u_2(\pi, \pi, \pi)$ plane. (See also Fig 10(g) which plots the three coordinates.) Even after the phase point has pierced the Poincaré plane a large number of times (8 or 10), each section consists of a single point.



(a) $Re_a = 6.24$ or $\chi = 0.3$. Simple periodic flow. \times Poincaré plane pierced from positive side. \bullet plane pierced from negative side.

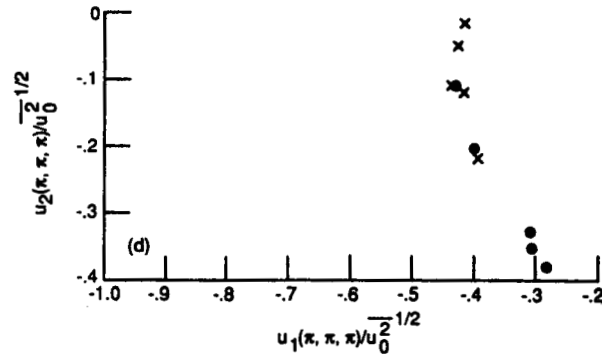


(b) Plane pierced from positive side, $Re_a = 6.72$ or $\chi = 0.338$.

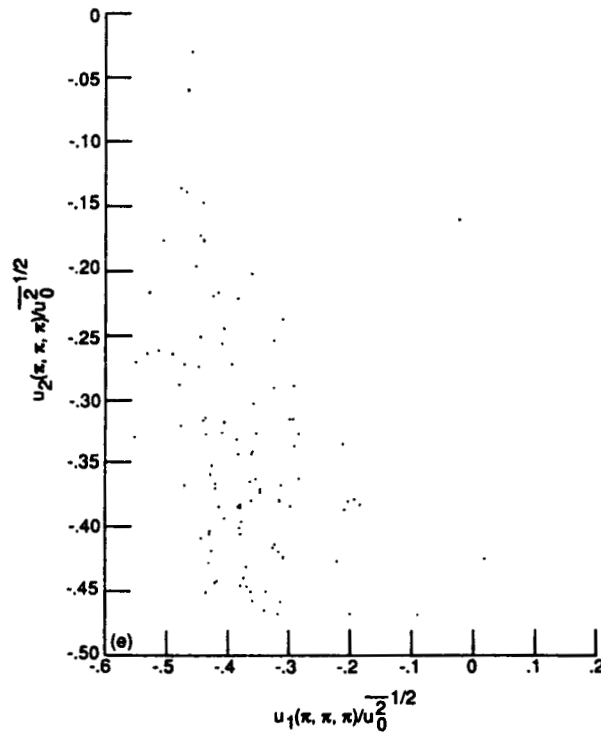


(c) Plane pierced from negative side, $Re_a = 6.72$ or $\chi = 0.338$.

Figure 11. - Poincaré sections of attractors.

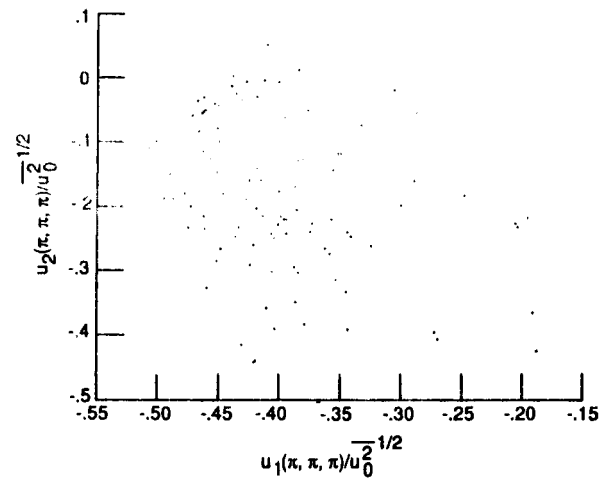


(d) $Re_a = 6.89$ or $\chi = 0.35$. Complex periodic flow. \times plane pierced from positive side. \bullet plane pierced from negative side.

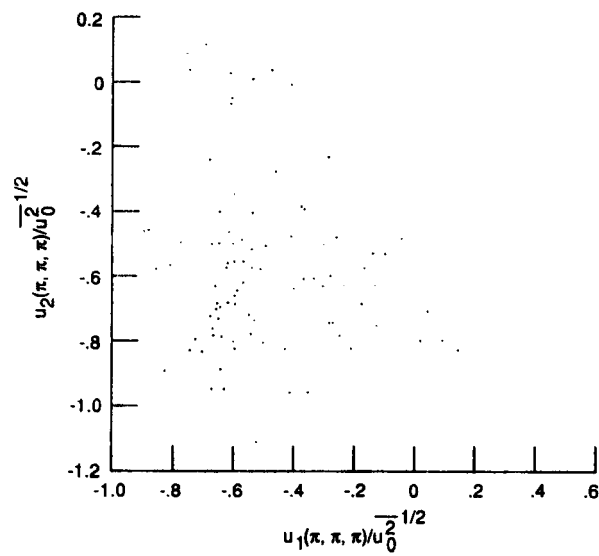


(e) Plane pierced from negative side. $Re_a = 6.93$ or $\chi = 0.4$.

Figure 11 continued.

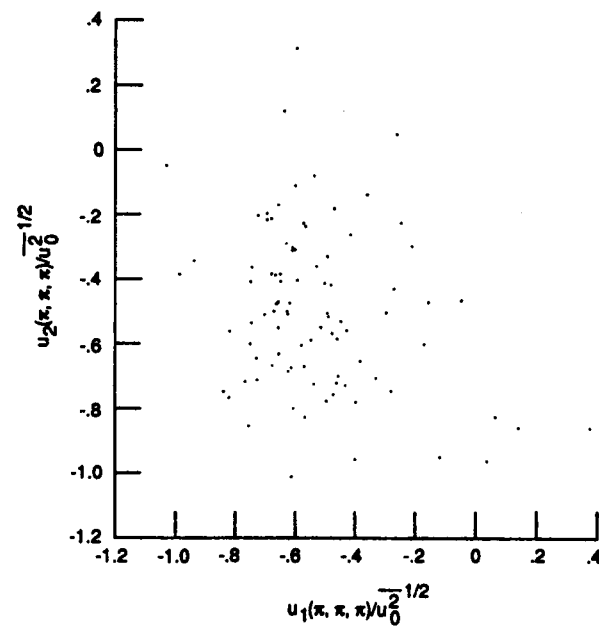


(f) Plane pierced from positive side. $Re_a = 6.93$ or $\chi = 0.4$



(g) Plane pierced from negative side. $Re_a = 13.3$ or $\chi = 1$.

Figure 11 continued.



(h) Plane pierced from positive side. Re_a 13.3 or $x = 1$.

Figure 11 concluded.

Consider next some Poincaré sections of the phase portrait for Figs. 10(i) to (o) ($\chi = 0.338$). These are plotted in Figs. 11(b) and (c). Some portions of the plots appear to be lines; that tends to indicate quasiperiodicity of the flow (with two independent frequencies). However, in other parts of the plots the points are scattered somewhat randomly with no apparent pattern; that tends to indicate chaos. Thus the flow has both chaotic and quasiperiodic features. It is not periodic because longer running times produce more points on the Poincaré section.

Two Poincaré sections for the complex periodic attractor of Figs. 10(p) to (r) are plotted in Fig. 11(d). These sections are similar to those in Fig. 11(a), but because of the complexity of the attractor of Figs. 10(p) to (r), each section consists of five points instead of one. As was the case for the simpler periodic attractor, the number of points does not increase with increasing running time.

Finally, in Figs. 11(e) to (h), we consider Poincaré sections for our two highest Reynolds-number flows ($\chi = 0.4$ and 1). Phase portraits for these flows were considered in Figs. 10(s) to (v). These Poincaré sections are similar to those in Figs. 11(b) and (c) insofar as longer running times produce more plotted points. However they are qualitatively different, since there are no regions where the points lie along a curve. They tend to fill a region of space in an apparently random fashion; there is no evident pattern.

D. Liapunov exponent

The Liapunov characteristic exponent (or largest Liapunov exponent if a spectrum of exponents is considered) provides a definitive way of determining whether or not a flow is chaotic. A positive Liapunov exponent indicates sensitive dependence on initial conditions, which in turn is often considered as synonymous with chaoticity.

The method used here to determine the sensitivity of our solutions to small changes in initial conditions, and to determine Liapunov exponents, is similar to one we used previously.⁸ The values of u_i at a time after initial transients have died out are perturbed by small spatially random numbers R , where $-10^{-6} < R < 10^{-6}$ or $-10^{-4} < R < 10^{-4}$. The perturbations are applied at each spatial grid point at one time. The distance between the perturbed and unperturbed solutions at various times is then calculated from

$$D = \left(\sum_{i,j} [u_{i,\text{perturbed}}(x_j, t) - u_{i,\text{unperturbed}}(x_j, t)]^2 \right)^{1/2} \quad (8)$$

where i , which can have values from 1 to 3, indicates different directional velocity components, and j , which can go from 1 to some number M , indicates different points in physical space. Then D represents a distance or norm in a $3M$ -dimensional space. For M equal to the number of grid points, D is the distance in the phase space of the discretized system. (Note that the distance D has the dimensions of a velocity.)

In reference 8, D was represented by embedding it in one-, three-, six-, and twelve-dimensional spaces. It was found that increasing the embedding dimension from three to twelve had little or no effect on the calculated value of the Liapunov exponent. Here we adopt six dimensions as giving a sufficiently good representation of D . That is, we use three velocity components at each of two points in physical space as the dimensions ($M = 2$).

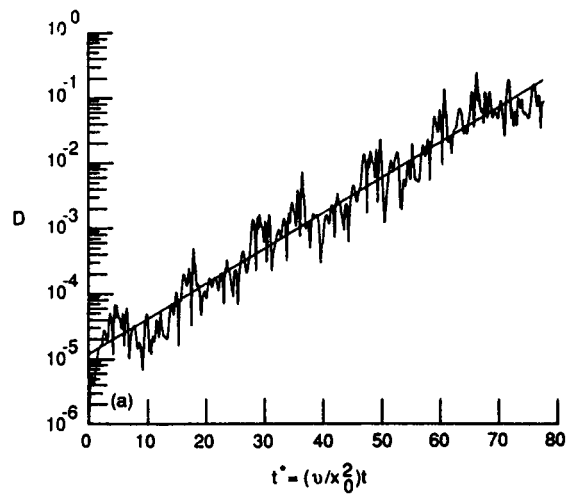
Thus, embedding the distance between perturbed and unperturbed solutions in a six-dimensional space and plotting $\log (D/u_0^2)^{1/2}$ against dimensionless time, we obtain Figs. 12(a) to (c) for $x = 0.338, 0.4$, and 1 . The values of $\log D$, on the average, increase linearly with time, indicating that D increases exponentially. That is, initially neighboring solutions diverge exponentially on the average. Thus it appears that we can characterize these three flows as chaotic.

The fact that the mean slopes of the distance-evolution curves are constant over a considerable range also allows us to use our results to obtain an estimate of the Liapunov characteristic exponent. The Liapunov characteristic exponent σ (for times after initial transients have died out) is defined as⁶

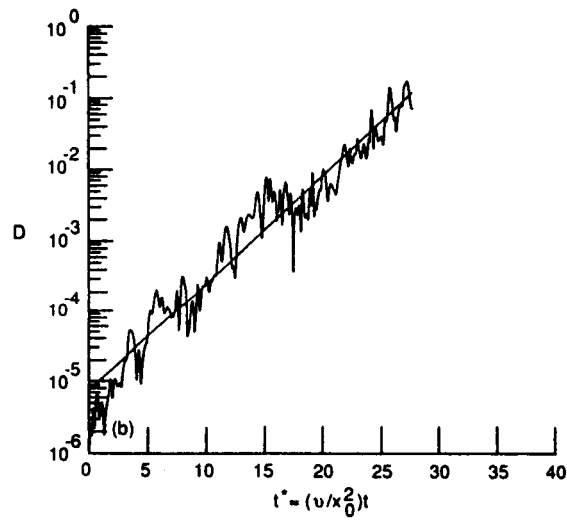
$$\sigma = \lim_{\substack{t \rightarrow \infty \\ D(0) \rightarrow 0}} \left(\frac{1}{t} \right) \ln \frac{D(t)}{D(0)}, \quad (9)$$

where the $D(t)$ are values of distance between initially neighboring solutions that might be obtained from Fig. 12.

However, if the values of D were obtained from the wavy curves

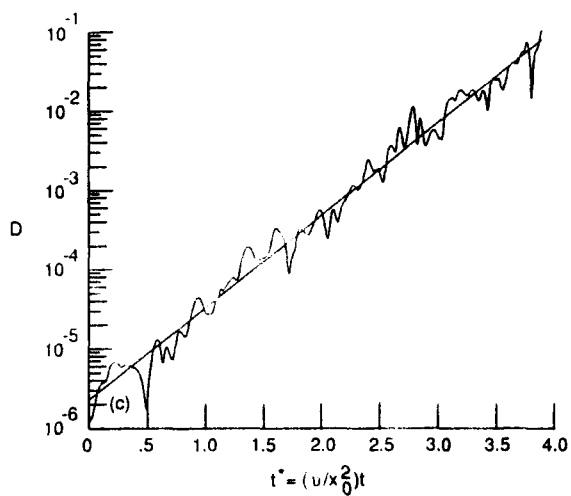


(a) $Re_a = 6.72$ or $\lambda = 0.338$. $-10^{-6} < R < 10^{-6}$. Chaotic flow.

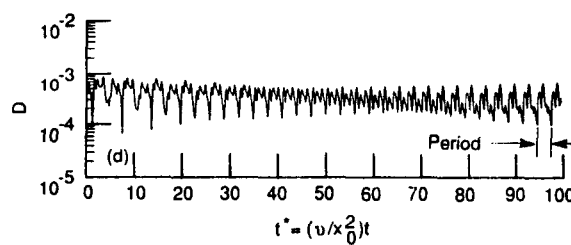


(b) $Re_a = 6.93$ or $\lambda = 0.4$. $-10^{-6} < R < 10^{-6}$. Chaotic flow.

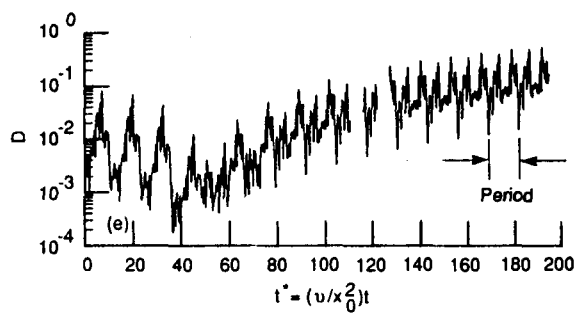
Figure 12. - Semilogarithmic plots showing evolution of distance D between neighboring solutions.



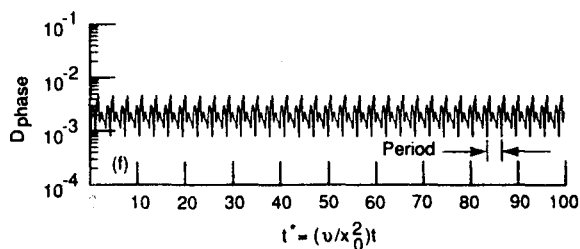
(c) $Re_a = 13.3$ or $\lambda = 1$. $10^{-6} < R < 10^{-5}$. Chaotic flow.



(d) $Re_a = 6.24$ or $\lambda = 0.3$. $10^{-4} < R < 10^{-3}$. Simple periodic flow.

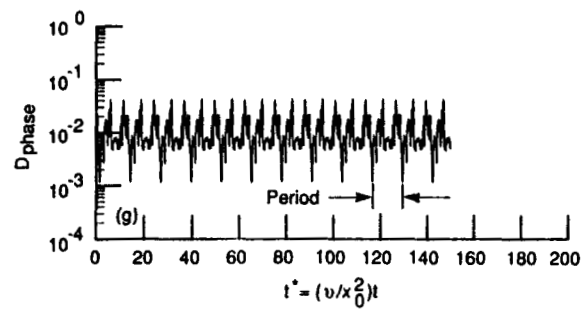


(e) $Re_a = 6.89$ or $\lambda = 0.35$ Complex periodic flow.



(f) Separation distance if phase point is perturbed only along trajectory. $Re_a = 6.24$ or $\lambda = 0.3$. Simple periodic flow.

Figure 12. - Semilogarithmic plots showing evolution of distance D between neighboring solutions.



(g) Separation distance if phase point is perturbed only along trajectory. $Re_a = 6.89$ or $\lambda = 0.35$. Complex periodic flow.

Figure 12 concluded.

in Fig. 12, we would have to go to very large times in order to obtain a reasonable estimate for σ . This would take us out of the region of exponential growth of D , unless $D(0)$ were very small (probably below the computer noise level). One way of getting around this difficulty is to use a renormalization procedure.⁶

For our purposes it seems that, since the mean slopes of the distance evolution curves in Fig. 12 are constant over a considerable range, the best procedure is to replace the wavy curves by straight lines through them. Then Eq. (9) is replaced by

$$\sigma = [\ln (D_m/D_a)]/(t - t_a), \quad (10)$$

where the values of D_m and D_a are read from the straight line in each figure at times t and t_a , respectively. The straight line in each figure is drawn so that its mean square deviation from the wavy curve is a minimum; this procedure should give a good estimate for σ . The values of dimensionless σ so obtained for Figs. 12(a) to (c) are, respectively,

$$\left(x_0^2/\nu\right)\sigma \approx 0.12, \quad 0.35, \quad \text{and} \quad 2.7. \quad (11)$$

The value 2.7 agrees with that obtained for the same flow (but for a different time of perturbation and different embedding dimension) in reference 8. The Liapunov exponents in Eq. (11) give us a measure of the mean exponential rate of divergence of two initially neighboring solutions, or of the chaoticity of the flows. The important point is that σ is positive, indicating

that these three flows are chaotic.⁶ It is noted that as the Reynolds number increases σ increases (for constant x_0 and v), or the flows become more chaotic.

Plots of dimensionless D versus t^* for our two periodic flows are given in Figs. 12(d) and (e). (Note two lost-data gaps in the Fig. 12(e) curve.) These plots are qualitatively different from those for chaotic flows. If they were not, of course, our method for calculating Liapunov exponents would be in error. Whereas D for chaotic flow increases exponentially (on the average) for about four orders of magnitude until it is of the same order as u_1 , D for the periodic flows, on the average, shows no tendency to increase exponentially. Thus the Liapunov exponent does not show a tendency to be positive, as of course it should not, since the flow is not chaotic. Theoretically the largest Liapunov exponent, the one associated with perturbations along a trajectory, should be zero for a periodic attractor.¹⁴

The following simple argument shows that the largest Liapunov exponent for a limit cycle is zero. A limit cycle is *stable*, so the flow must return to the same periodic attractor after a perturbation. That is, the trajectory, a long time after perturbation, must occupy the same points in phase space as it did before perturbation. So the only possible difference between the perturbed and unperturbed trajectories is that there may be a phase difference; although the trajectory, a long time after perturbation, must occupy the same points in phase space as does

the unperturbed trajectory, it may do so at different times. A phase difference is allowable because our dynamical system is autonomous; time does not appear on the right side of Eq. (1). Since the velocity components are all periodic in time, D will be periodic, as in Figs. 12(f) and (g). There the limit cycle is perturbed along its trajectory by introducing a small phase difference Δt ; the distance between neighboring solutions is calculated from

$$D_{\text{phase}} = \left(\sum_{i,j} [u_i(\mathbf{x}_j, t + \Delta t) - u_i(\mathbf{x}_j, t)]^2 \right)^{1/2} \quad (12)$$

in place of Eq. (8). Thus the average D over a long time has zero slope, so that for a periodic flow, the largest Liapunov exponent (associated with perturbations along the trajectory) is zero. Other Liapunov exponents (associated with perturbations normal to the trajectory) are negative, since the flow is attracted to the limit cycle. Note that Figs. 12(f) and (g) do not by themselves, without the rest of the above argument, show that the largest Liapunov exponent is zero. However the wavy curves in Figs. 12(d) and (e) do approach those in Figs. 12(f) and (g) respectively for very long times. In particular the wavy-curve shape in Fig. 12(g) is nearly identical with that near the end of the curve in Fig. 12(e). So the use of Eq. (12) is a way of producing the asymptotic D 's immediately when it is known that the asymptotic D 's are the result of a phase difference, or

of a perturbation along the trajectory. The effects of perturbations normal to the trajectory are absent in Figs. 12(f) and (g).

E. Characterization of the flow for $\chi = 0.338$

The fact that the flows for Figs. 12(b) and (c) are chaotic might be expected from the lack of a pattern in the time series, phase portraits, and Poincaré sections for those flows. On the other hand the flow for Fig. 12(a) ($\chi = 0.338$) has both chaotic and quasiperiodic features, as shown particularly by the Poincaré sections in Figs. 11(b) and (c). (A flow for $\chi = 0.341$ (not shown) also has those features.) Because of the positive Liapunov exponent of the flow for $\chi = 0.338$ in Fig. 12(a) we classify that flow as chaotic. But we should differentiate between the $\chi = 0.338$ flow (Figs. 11(b) and (c)) and the flows for $\chi = 0.4$ and 1 (Figs. 11(e) to (h)) because of the qualitative difference between their Poincaré sections. Since the Poincaré sections for the $\chi = 0.338$ flow do not show a complete lack of pattern, we call it weakly chaotic to distinguish it from the $\chi = 0.4$ and 1 flows which we call fully chaotic or simply chaotic.

F. Chaotic versus turbulent flows

This leads us to a possible distinction between flows which are chaotic and those which, in addition, might be called turbulent. Perhaps one should reserve the term "turbulent" for flows which have both a positive Liapunov exponent and Poincaré

sections with a lack of pattern, as have those for $x = 0.4$ and 1. On the other hand chaotic flows (albeit weakly chaotic) might have only a positive Liapunov exponent.

Another characteristic which is often given as indicative of turbulence is a negative skewness factor S of the velocity derivative, where usually $-1 < S < 0$.¹² However, for the time-dependent flows considered here, both turbulent and nonturbulent, the skewness factor did not vary significantly from that given in Eq. (7). Even for the fixed-point flow (Figs. 9(a) and 10(a)) the value of S was about -0.25 . Thus although a negative S is necessary for the presence of turbulence, it is certainly not a sufficient indicator. A negative S in fact seems to be more an indicator of nonlinearity than of turbulence. All of the flows here are highly nonlinear.

G. Power spectra

Power spectra give the distribution with frequency of the energy in a flow. We obtain the spectra by computing the fast Fourier transforms of the time series for the velocity components. The squares of the absolute values of those transforms are then plotted against dimensionless frequency. The results are given in Fig. 13.

Two types of spectra are indicated—discrete for the periodic flows and continuous for the chaotic ones. However the spectra do not appear able to distinguish qualitatively between the weakly chaotic (Fig. 13(b)) and the fully chaotic flows (Figs. 13(d) and

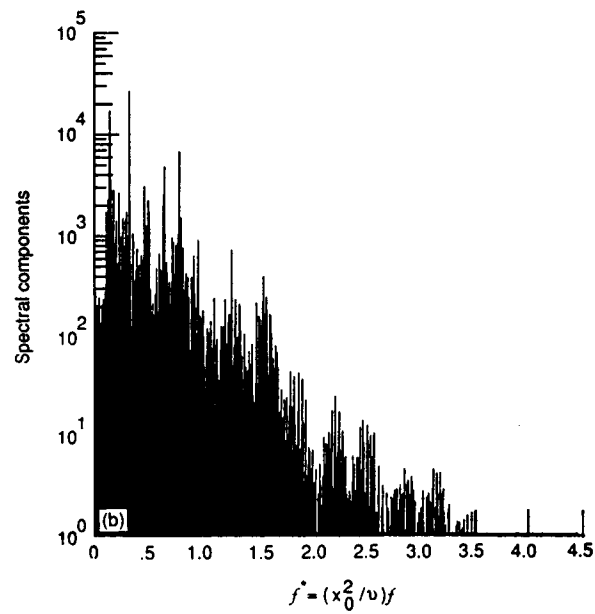
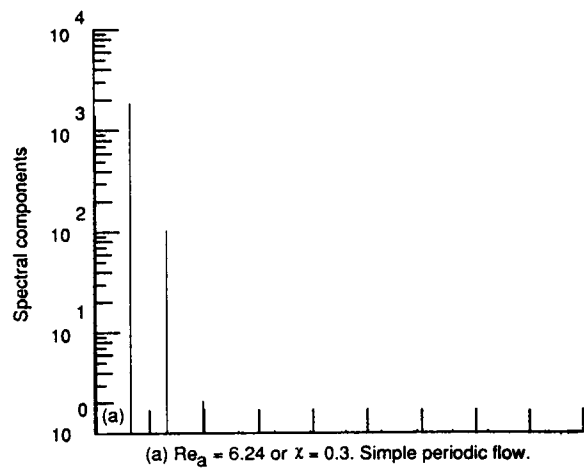


Figure 13. - Power Spectra.

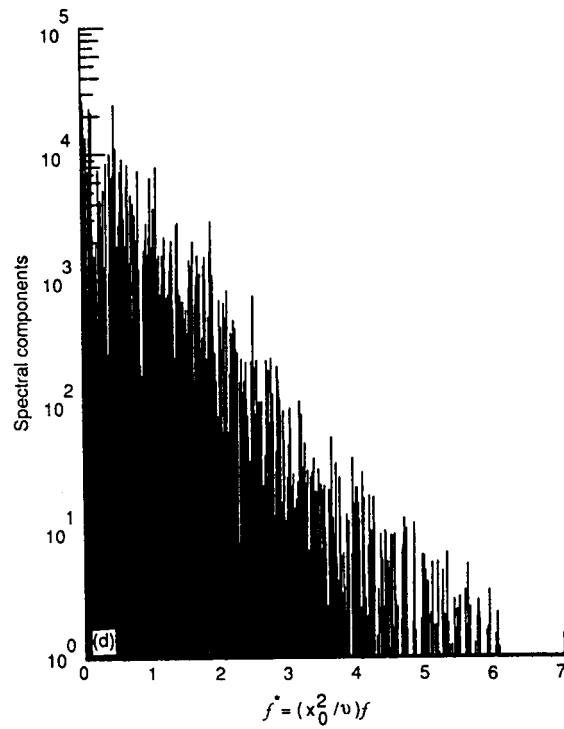
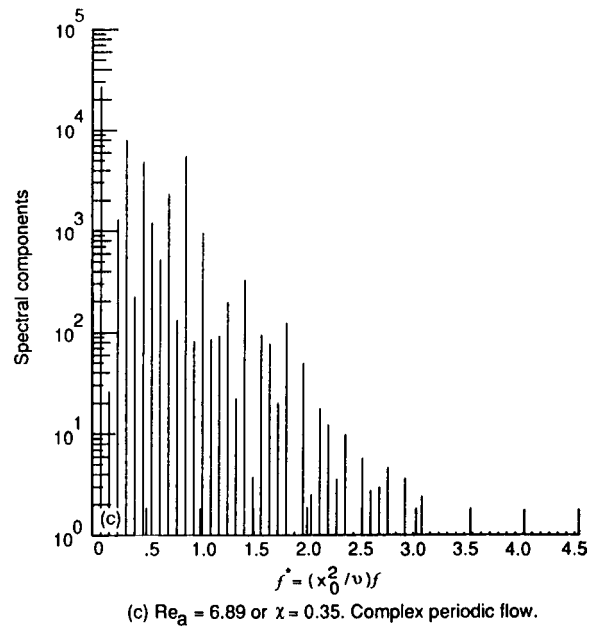


Figure 13

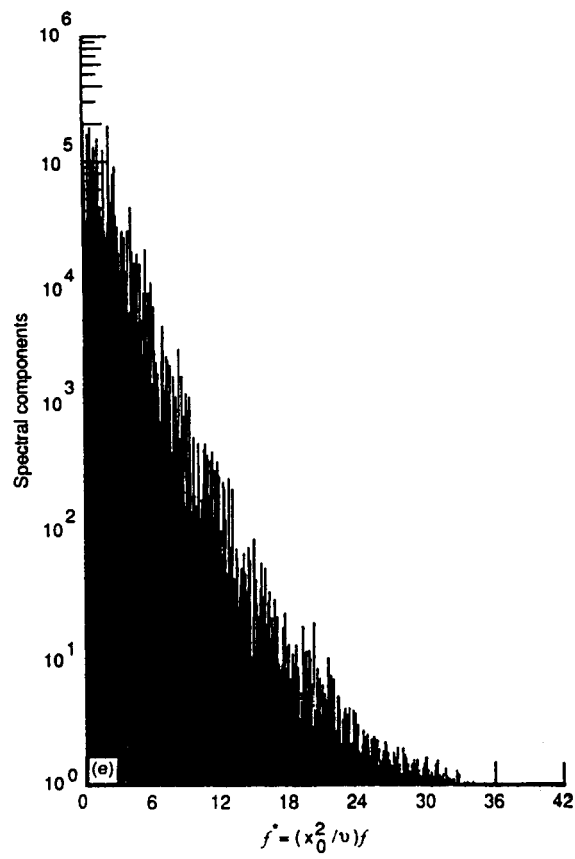


Figure 13 concluded.

(e)). In that respect they are less sensitive indicators than are the Poincaré sections. If one considers the discrete and continuous spectra separately, then higher frequency components become excited as the Reynolds number increases (as x increases). In the case of the discrete spectra, the simple periodic flow (Fig. 13(a)) requires only four spectral components to represent u_2 , whereas the much more complex periodic flow (Fig. 13(c)) requires 36 nonnegligible components. In both cases the frequencies of the components are related to one another as ratios of integers (one fundamental frequency in each case).

H. Dimensions of the attractors

As a final characterization of our Navier-Stokes flows, we consider the dimensions of the attractors on which the flows reside. The dimension of a space gives, in general, the number of quantities required to specify the position of a point in the space; e.g., one, two, or three coordinates are respectively required to specify a point in a one-, two-, or three-dimensional physical space. The same applies to an n -dimensional phase space, or to an attractor which is a portion of the phase space. The attractor is generally of lower dimension than that of the phase space because of the shrinking of volumes in the phase space of a dissipative system. It is partly this possibility of a decreased dimension of the attractor, and consequent simplification of the problem (in principle), which makes calculation of dimension an interesting pursuit. The dimension can be considered the lower

bound on the number of essential variables needed to describe the dynamics of a system.¹⁵ Unfortunately it is usually difficult to obtain reliable estimates of that quantity.

As mentioned in section III.B, the dimensions of our fixed-point and periodic attractors are respectively zero and one; a point in any space is zero-dimensional and a closed line, no matter how complicated its shape, is one-dimensional if the optimum coordinate system or basis function is used (see discussion in section III.B).

One might question why more than one spectral component is required in Figs. 13(a) and (c) for the representation of one-dimensional periodic attractors. However the need for more than one component in those representations means only that the basis functions used there, sines and cosines, are not optimum for those cases. In the case of our complex periodic flow (Fig. 13(c)) it would be necessary to use an extremely complicated basis function for one-spectral-component representation—most likely a basis function represented numerically rather than by an analytical function.

We also attempted to calculate the pointwise dimensions of our chaotic or strange attractors.^{15,16} In that attempt we have not been able to obtain a long enough time series for the dimension to become independent of time-series length. Thus, all we can say with certainty is that the dimension must be greater than 2; if it were not, trajectories for our chaotic flows would cross in phase space. They cannot cross for an autonomous system because if they

did, there would be more than one trajectory for the same conditions (at the point where the trajectories cross), and the problem would not be deterministic.

One might expect that for our weakly chaotic flow the dimension would be only slightly greater than 2 because apparent folding can be seen in the phase portrait (Figs. 10(j) and (m)); if the attractor were many-dimensional, stretching and folding would occur in many directions and, because of the resulting confusion, could not be discerned in a two-dimensional plot. That is apparently what happens for the fully chaotic flows (Figs. 10(s) to (v)). There the dimension must be significantly greater than 2; stretching and folding, although certainly present, is many-dimensional, so that the result is a confused appearance of the phase portrait. However, even there the dimension of the attractor should be limited by the overall shrinkage of volumes in phase space.

IV. TURBULENT ENERGY TRANSFER AND TURBULENT DISSIPATION

Thus far we have used only the unaveraged equations of motion, those being the most useful for analyzing turbulence by using tools of nonlinear dynamics. On the other hand, for discussing the transfer of energy between wavenumbers or between directional components, or turbulent dissipation, averaged or moment equations have traditionally been used.¹ Here we will use both averaged and unaveraged equations. Spectral transfer by nonlinear self-interaction and by the interaction of turbulence with a mean velocity gradient, as well as directional transfer of energy, and turbulent dissipation, are central to the nature of turbulence and so are discussed here.

First we show that energy transfer and dissipation are generic in Navier-Stokes turbulence, where the turbulence can be statistically homogeneous or inhomogeneous. Turbulence must be dissipative, since the Navier-Stokes equations form a dissipative system. But it requires some analysis to show that energy transfer, particularly spectral transfer in nonhomogeneous turbulence, is generic.¹⁷

We write the incompressible Navier-Stokes equation at two points P and P' separated by the vector \mathbf{r} (see Fig. 14). If we break the instantaneous velocity and pressure into mean and fluctuating components, we can construct the following two-point correlation equation:¹⁷

$$\begin{aligned}
\frac{\partial \overline{u_i u_j}}{\partial t} = & - \overline{u_k u_j} \frac{\partial \overline{u_i}}{\partial x_k} - \overline{u_i u_k} \frac{\partial \overline{u_j}}{\partial x_k} - \overline{u_k} \frac{\partial \overline{u_i u_j}}{\partial x_k} - \overline{u_k} \frac{\partial \overline{u_i u_j}}{\partial x_k} \\
& - \frac{\partial}{\partial x_k} \overline{u_i u_k u_j} - \frac{\partial}{\partial x_k} \overline{u_i u_j u_k} - \frac{1}{\rho} \left(\frac{\partial \overline{p u_i}}{\partial x_i} + \frac{\partial \overline{p u_j}}{\partial x_j} \right) + \nu \left(\frac{\partial^2 \overline{u_i u_j}}{\partial x_k \partial x_k} + \frac{\partial^2 \overline{u_i u_j}}{\partial x_k' \partial x_k'} \right),
\end{aligned}
\tag{13}$$

where the subscripts can take on the values 1, 2, or 3, and a repeated subscript in a term indicates a summation on the subscript. The unprimed quantities are measured at point P, and the primed quantities at P', as in Fig. 14. The overbar designates an averaged quantity. The quantity u_i is a fluctuating velocity component ($\overline{u_i} = 0$), $\overline{U_i}$ is a mean velocity component, p is the fluctuating pressure, ρ is the density, ν is the kinematic viscosity, x_i is a space coordinate, and t is the time. Referring to Fig. 14,

$$x + r = x', \quad x + nr = x_n,$$

from which

$$x_n = nx' + (1 - n)x.$$

In subscript notation,

$$r_k = x_k - x_k, \tag{14}$$

and

$$(x_k)_n = nx_k + (1 - n)x_k, \tag{15}$$

where n is a number between 0 and 1. By using Eqs. (14) and (15) and the rules for partial differentiation, we obtain

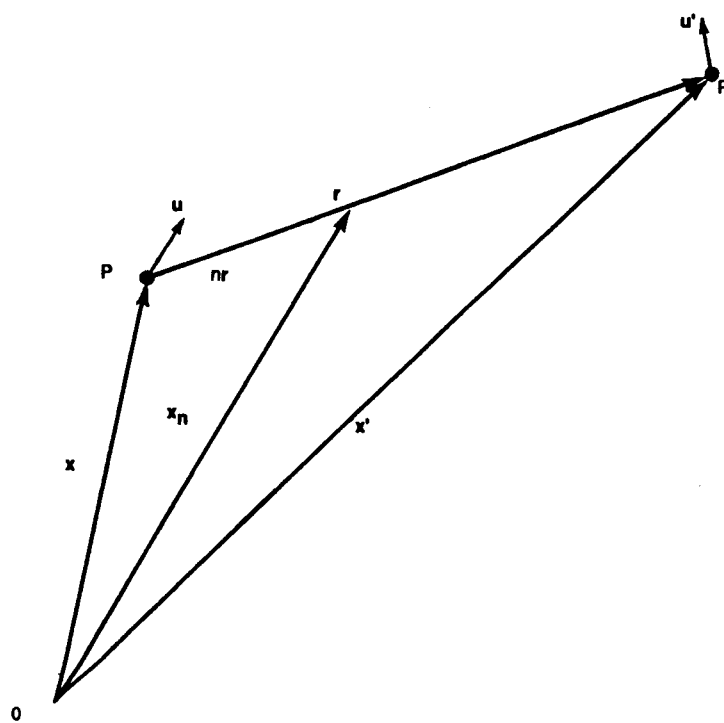


Figure 14. - Vector configuration for two-point correlation equation.

$$\frac{\partial}{\partial x_k} = (1 - n) \frac{\partial}{\partial (x_k)_n} - \frac{\partial}{\partial r_k}, \quad (16)$$

and

$$\frac{\partial}{\partial x'_k} = n \frac{\partial}{\partial (x_k)_n} + \frac{\partial}{\partial r_k}. \quad (17)$$

Equations (16) and (17) are used to transform, except in the last two terms, the independent variables in Eq. (13) from x_k and x'_k to $(x_k)_n$ and r_k :

$$\begin{aligned} \frac{\partial \overline{u_i u_j}}{\partial t} = & - \frac{\partial}{\partial r_k} (\overline{u_i u_j u'_k} - \overline{u_i u_k u'_j}) - (U'_k - U_k) \frac{\partial}{\partial r_k} \overline{u_i u_j} \\ & - \frac{\partial}{\partial (x_k)_n} [(1 - n) \overline{u_i u_k u'_j} + n \overline{u_i u'_j u'_k}] \\ & - [(1 - n) U_k + n U'_k] \frac{\partial}{\partial (x_k)_n} \overline{u_i u'_j} + P_{ij} - \frac{1}{\rho} \left(\frac{\partial \overline{p u'_j}}{\partial x_i} + \frac{\partial \overline{u_i p'}}{\partial x'_j} \right) \\ & + \nu \left(\frac{\partial^2 \overline{u_i u_j}}{\partial x_k \partial x_k} + \frac{\partial^2 \overline{u_i u'_j}}{\partial x'_k \partial x'_k} \right) \end{aligned} \quad (18)$$

where the two terms containing $\partial/\partial (x_k)_n$ are, respectively, the diffusion and convection terms, P_{ij} is the production term, and the last two terms are respectively the pressure and dissipative terms.

Consider the first term on the right side of Eq. (18), the turbulence self-interaction term. We can write

$$- \frac{\partial}{\partial r_k} (\overline{u_i u'_j u'_k} - \overline{u_i u_k u'_j}) = \int_{-\infty}^{\infty} T_{ij}(\kappa, x_n) \exp(i\kappa \cdot r) d\kappa, \quad (19)$$

where T_{ij} is the three-dimensional Fourier transform of $-(\partial/\partial r_k)(\overline{u_i u_j' u_k'} - \overline{u_i u_k' u_j'})$, κ is the wavenumber vector, and $d\kappa = d\kappa_1 d\kappa_2 d\kappa_3$. As in a homogeneous turbulent velocity field, $\partial(\overline{u_i u_j' u_k'} - \overline{u_i u_k' u_j'})/\partial r_k$ for an inhomogeneous field should be absolutely integrable over r in order for its Fourier transform to exist. Moreover, if a wall is present in the flow, a finite Fourier transform with respect to the component of r normal to the wall should be used. We want to determine whether T_{ij} can be interpreted as a spectral-transfer term. To this end we solve Eqs. (17) and (16) for $\partial/\partial r_k$ and write Eq. (19) as

$$\begin{aligned} \int_{-\infty}^{\infty} T_{ij}(\kappa, x_n) \exp(i\kappa \cdot r) d\kappa &= -\frac{\partial}{\partial r_k} \overline{u_i u_j' u_k'} + \frac{\partial}{\partial r_k} \overline{u_i u_k' u_j'} \\ &= \left(-\frac{\partial}{\partial x_k'} + n \frac{\partial}{\partial (x_k)_n} \right) \overline{u_i u_j' u_k'} + \left(-\frac{\partial}{\partial x_k} + (1-n) \frac{\partial}{\partial (x_k)_n} \right) \overline{u_i u_k' u_j'} \\ &= -\overline{u_i u_k' \frac{\partial u_j'}{\partial x_k'}} - \overline{u_j' \frac{\partial}{\partial x_k} u_i u_k} + \frac{\partial}{\partial (x_k)_n} \left(n \overline{u_i u_j' u_k'} + (1-n) \overline{u_i u_k' u_j'} \right) \quad (20) \end{aligned}$$

where the continuity condition $\partial u_k / \partial x_k = 0$ and the fact that quantities at one point are independent of the position of the other point were used. Equation (20) becomes, for $r = 0$,

$$\begin{aligned} \int_{-\infty}^{\infty} T_{ij}(\kappa, x_n) d\kappa &= - \left(\overline{u_i u_k' \frac{\partial u_j'}{\partial x_k}} + \overline{u_j' \frac{\partial}{\partial x_k} u_i u_k} \right) + \frac{\partial}{\partial x_k} \overline{u_i u_j' u_k} \\ &= -\frac{\partial}{\partial x_k} \overline{u_i u_j' u_k} + \frac{\partial}{\partial x_k} \overline{u_i u_j' u_k} = 0, \quad (21) \end{aligned}$$

since, for $r = 0$, $x_k = x'_k = (x'_k)_n$. Therefore, even for a general inhomogeneous turbulence, T_{ij} , when integrated over all wavenumbers, gives zero contribution to the rate of change of $u_i u_j$ (see Eqs. (18) and (19)). Thus, $T_{ij}(\kappa, x_n)$ can only transfer Fourier components of $u_i u_j$ (energy for $i=j$) from one part of wavenumber space to another.

The second term on the right side of Eq. (18), in contrast with the first (which produces turbulence self-interaction), is associated with the interaction of the turbulence with the mean flow. However, both terms are related to transfer terms. We can write

$$-(U'_k - U_k) \frac{\partial}{\partial r_k} \overline{u_i u'_j} = \int_{-\infty}^{\infty} T_{ij}^*(\kappa, x_n) \exp(i\kappa \cdot r) d\kappa, \quad (22)$$

where $T_{ij}^*(\kappa, x_n)$ is the Fourier transform of $-(U'_k - U_k)(\partial/\partial r_k) \overline{u_i u'_j}$.

Letting $r = 0$, Eq. (22) becomes

$$\int_{-\infty}^{\infty} T_{ij}^*(\kappa, x_n) d\kappa = 0 \quad (23)$$

since, for $r = 0$, $U'_k = U_k$. Thus, as in the case of $T_{ij}(\kappa, x_n)$, $T_{ij}^*(\kappa, x_n)$ gives zero total contribution to the rate of the change of $\overline{u_i u_j}$ (energy for $i = j$) and can only alter the distribution in wavenumber space of contributions to $\overline{u_i u_j}$. We first interpreted and calculated $T_{ij}^*(k)$ as a transfer term for homogeneous turbulence in reference 18. (Craya¹⁹ also discusses, in a general way, the modification of homogeneous turbulence by uniform mean gradients, but does not show that T_{ij}^* is specifically a spectral-transfer term.)

The first two terms on the right side of Eq. (18) appear to be the only ones associated with spectral transfer. The other terms are interpretable as production, convection, directional-transfer, diffusion, and dissipation terms. In particular the next to the last term is the directional-transfer term; using the continuity equation at the points P and P' and setting $i = j$ shows that the term gives zero contribution to the rate of change of $\overline{u_i u_i}$, but it can transfer energy among the directional components of $\overline{u_i u_i}$ (among $\overline{u_1 u_1}$, $\overline{u_2 u_2}$, and $\overline{u_3 u_3}$). Finally the last term, which is proportional to the viscosity, is the dissipation term.

Next we want to show how spectral transfer can take place by using results from simple analyses. For our purposes we consider the simplest closure scheme, the correlation-term-discard closure. In using that systematic procedure the infinite set of multipoint correlation equations is made determinate by neglecting the highest-order terms in the highest-order equations considered.^{18,20-22}

A. Homogeneous turbulence with no mean gradients

For this case we first use the two-point equation (26) from reference 20. That equation was obtained by neglecting the quadruple-correlation terms in the three-point correlation equation. Thus, we get, for the approach to the final period of decay (for weak turbulence),

$$\frac{dE}{dt} + 2\nu\kappa^2 E = T, \quad (24)$$

where

$$T(\kappa) = \int_0^\infty P(\kappa, \kappa') d\kappa' \quad (25)$$

and where

$$P(\kappa, \kappa') = - \frac{\beta_0}{2\nu(t - t_0)} (\kappa^5 \kappa'^7 - \kappa^7 \kappa'^5) \{ \exp[-2\nu(t - t_0)(\kappa^2 - \kappa\kappa' + \kappa'^2)] - \exp[-2\nu(t - t_0)(\kappa^2 + \kappa\kappa' + \kappa'^2)] \} \quad (26)$$

The quantity E is the energy spectrum function, related to the total turbulent energy $\overline{u_i u_i}/2$ by

$$\frac{1}{2} \overline{u_i u_i} = \int_0^\infty E(\kappa) d\kappa, \quad (27)$$

and $T(\kappa)$ is the energy transfer function, which equals $T(\kappa)/2$ integrated over all directions (see Eq. (19)). The term $-2\nu\kappa^2 E$ is the dissipation term. The quantities β_0 and t_0 are constants determined by the initial conditions. Then, carrying out the integration in Eq. (25) gives

$$T = - \frac{(\pi/2)^{1/2}}{256} \beta_0 \exp[-3/2\kappa^2\nu(t - t_0)] \left[105 \frac{\kappa^6}{(t - t_0)^{9/2}} + 45 \frac{\kappa^8}{(t - t_0)^{7/2}} - 19 \frac{\kappa^{10}}{(t - t_0)^{5/2}} - 3 \frac{\kappa^{12}}{(t - t_0)^{3/2}} \right], \quad (28)$$

and integration of Eq. (24) gives, with a particular set of initial conditions,²⁰

$$\begin{aligned}
E = & \frac{J_0 \kappa^4}{3\pi} \exp [-2v\kappa^2(t - t_0)] - \frac{\pi^{1/2} \beta_0}{256v} \exp [-3/2 \kappa^2 v(t - t_0)] \cdot \\
& \left[-\frac{15\sqrt{2}}{v^{7/2}} \frac{\kappa^6}{(t - t_0)^{7/2}} - \frac{12\sqrt{2}}{v^{5/2}} \frac{\kappa^8}{(t - t_0)^{5/2}} + \frac{7\sqrt{2}}{3v^{3/2}} \frac{\kappa^{10}}{(t - t_0)^{3/2}} \right. \\
& \left. + \frac{16\sqrt{2}}{3v^{1/2}} \frac{\kappa^{12}}{(t - t_0)^{1/2}} - \frac{32}{3} \kappa^{13} F\left(\kappa \left[\frac{v(t - t_0)}{2}\right]^{1/2}\right) \right] \quad (29)
\end{aligned}$$

where

$$\begin{aligned}
F(\omega) &= \exp(-\omega^2) \int_0^\omega \exp(x^2) dx, \\
\omega &= \kappa \left[\frac{v(t - t_0)}{2} \right]^{1/2},
\end{aligned}$$

and where J_0 is a constant determined by the initial conditions. Values of $F(\omega)$ are tabulated by Miller and Gordon.²³ The first term on the right side of Eq. (29) is the usual expression for E in the final period of decay. The last term is the contribution to E due to energy transfer.

Figure 15 shows the evolution of calculated energy spectra, where the dimensionless $E^* = J_0^{1/3} E / v^{8/3}$ is plotted against $\kappa^* = J_0^{1/3} \kappa / v^{2/3}$. The wavenumber κ has the dimension 1/length and can be considered as the reciprocal of an eddy size. Large wavenumbers therefore correspond to small eddies and small wavenumbers, to large eddies. Equation (27) shows that E represents the distribution of contributions to the total energy from various wave numbers or eddy sizes. As time increases, the

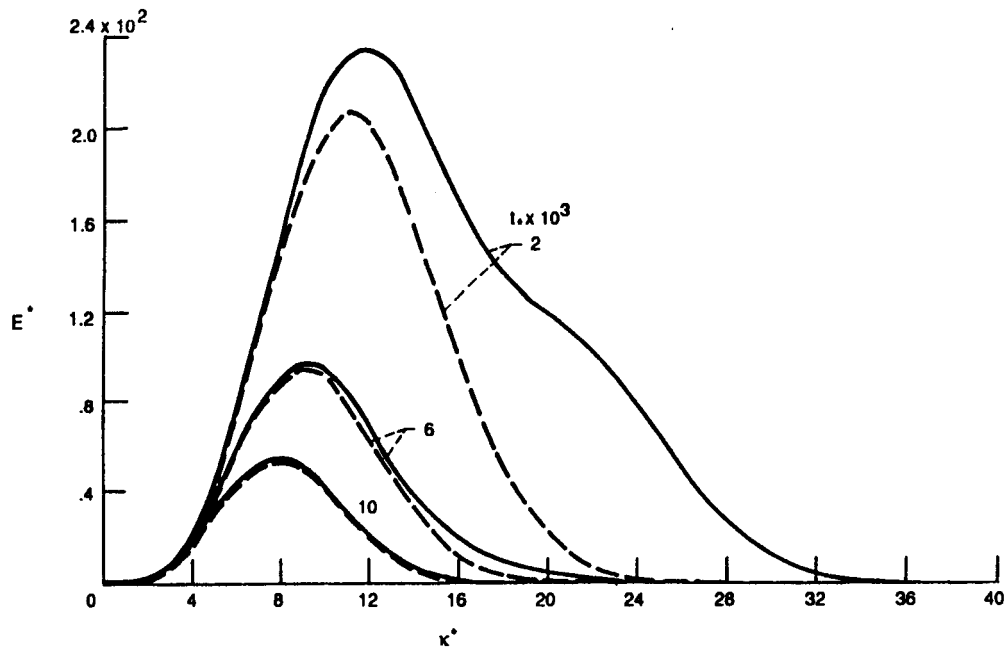


Figure 15. - Evolution of calculated energy spectra with $t_* = (\nu^{7/3}/J_0^{2/3})t$, $\theta_0 = \nu^5 B_0/J_0^4 = 1.55 \times 10^{-11}$,
 $t_0 = (\nu^{7/3}/J_0^{2/3})t_0 = -6.33 \times 10^{-3}$. — before final period ((Eq. (29)), - - - final period.

bulk of the energy moves to smaller wavenumbers or to larger eddies. The high velocity gradients and, consequently, high shear stresses occurring in the smaller eddies cause them to dissipate more rapidly than the larger ones. The form of the dissipation term $-2\nu\kappa^2 E$ in Eq. (24) also shows that the dissipation should be higher at the higher wavenumbers. The viscous dissipation thus produces a sink for the energy at the higher wavenumbers.

Also given in Fig. 15 is a comparison between spectra for times before the final period as obtained from Eq. (29), and those for the final period of decay obtained by neglecting the terms in brackets in Eq. (29). The difference is, of course, caused by the transfer of energy from low wavenumbers to higher ones by the transfer term T in Eq. (24). The energy transferred tends to fill the sink produced by dissipation at the higher wavenumbers. That causes the slopes on the high wavenumber sides of the spectra to be more gradual than in the final period. The effect is also observed experimentally.¹

The effect of the transfer term on the energy spectrum might be summarized by saying that it excites the higher wavenumber regions of the spectrum by transferring energy into those regions. The high wavenumber portion of the spectrum is thus determined primarily by inertia effects, whereas the low wavenumber portion is determined by the viscous terms in the equations. This may seem to contradict what we said before, where we mentioned that viscous dissipation is highest in the high wavenumber region.

However, the small eddies owe their existence in the first place to the transfer of energy into that region, that is, to inertia effects.

Figure 16 shows the dimensionless energy transfer term T^* (see Eq. (24)) plotted against κ^* for several values of $t_* - t_0^*$. The transfer term gives the net energy transfer into a wavenumber band from all other wavenumbers (see Eq. (25)). The curves indicate net energy loss from energy bands at low wavenumbers and an energy gain to those at higher wavenumbers. The total area under each curve is zero, in agreement with Eq. (21), thus indicating that the total contribution of T to $\overline{\partial u_i u_i} / \partial t$ is zero (see Eqs. (24) and (27)). It should be emphasized that T represents a difference between the energy flowing into and out of a wavenumber band. The actual energy transfer at a point where T is low or zero may be quite high, as will be shown.

Equation (25) shows that $P(\kappa, \kappa')$ gives the distribution of contributions to $T(\kappa)$ from various wavenumbers κ' . According to the present analysis $P(\kappa, \kappa')$ is given by Eq. (26).

In Fig. 17 we plot dimensionless P against κ' / κ for values of $\kappa[\nu(t - t_0)]^{1/2}$ corresponding to T a maximum and to $T = 0$. The curves indicate that the energy entering a wavenumber band at κ comes from a range of wavenumbers κ' (or eddy sizes) rather than primarily from neighboring wavenumbers. Similarly the energy passes to a range of wavenumbers. Thus the energy in general is

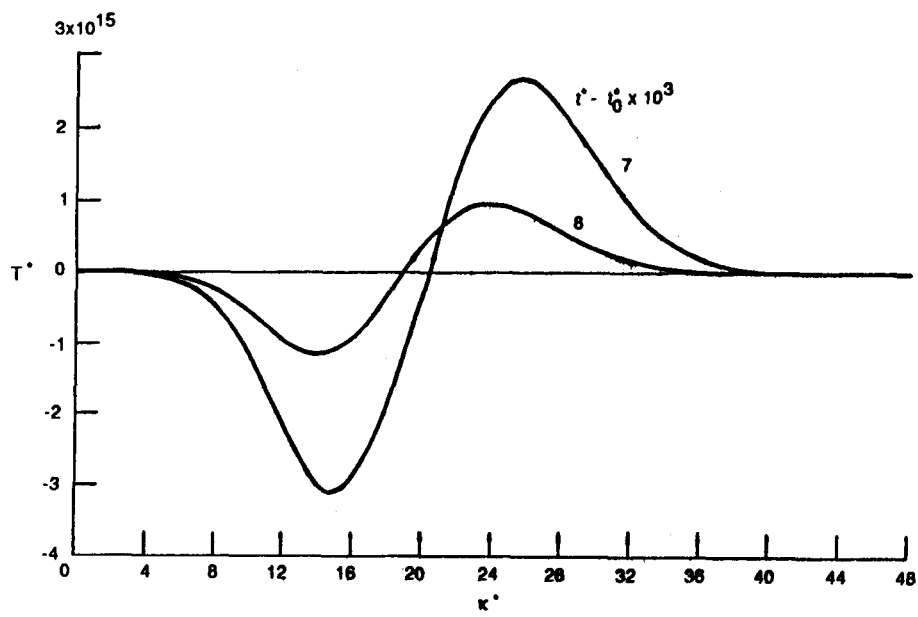


Figure 16. - Variation of dimensionless energy transfer term $T^* = J_0^5 T / (v^{10} B_0)$ with κ^* and $t^* - t_0^*$.

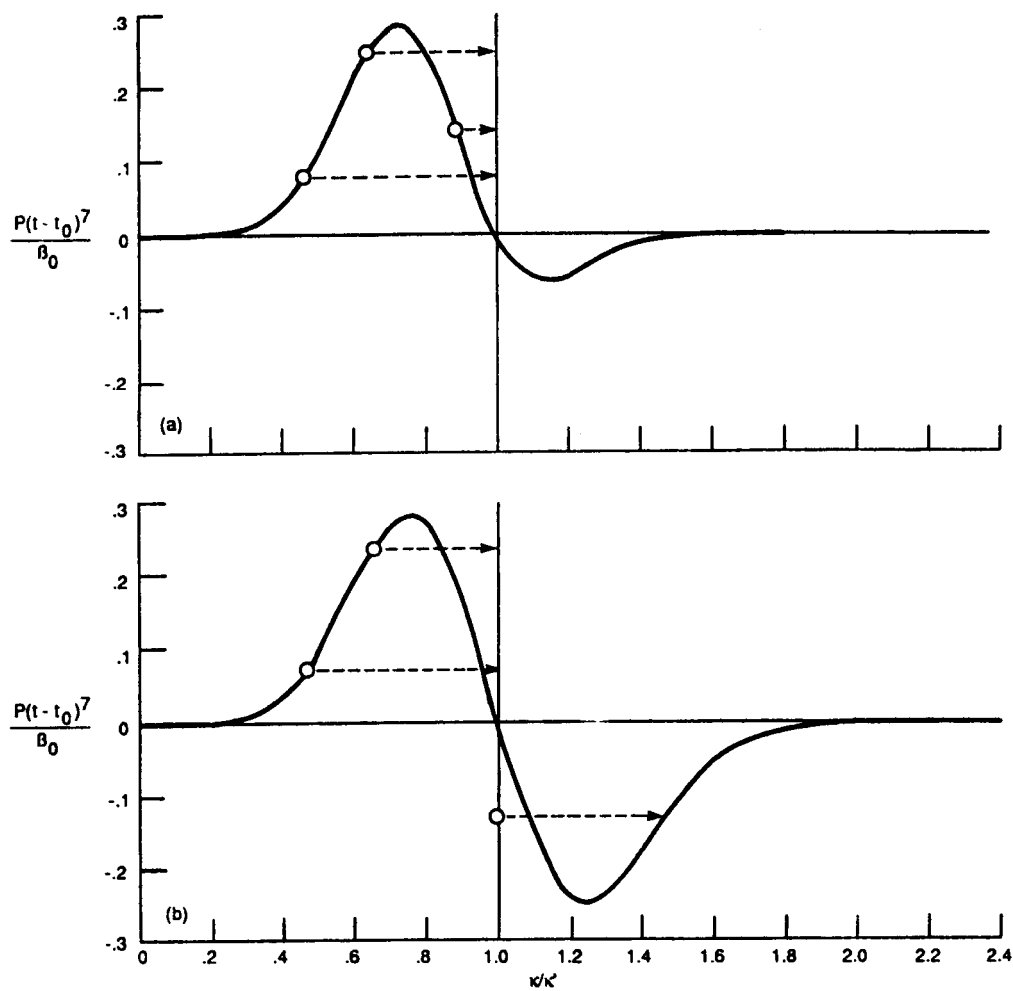


Figure 17. - Plots showing contributions to energy transfer at κ from various wave numbers κ' . $\bigcirc \rightarrow$ Energy transfers (jumps) from several κ' to κ , or from κ to several κ' . (a) T , a maximum; (b) $T=0$.

transported between wavenumber bands that are separated. This transport might occur by a breaking up of large eddies into smaller ones. The positive area under each curve corresponds to the total energy entering a wavenumber band at κ , the negative area to the total energy leaving. The curve for $T = 0$ indicates a considerable amount of energy entering and leaving at κ , although the net energy gain is zero.

Figures 15 to 17 give a picture of the energy transfer in the weak turbulence before the final period of decay. Figure 18 gives the results of an approximate calculation²⁴ of contributions $P(\kappa, \kappa')$ to experimental energy transfer $T(\kappa)$.²⁵ The turbulence is stronger than that before the final period. Still stronger turbulence²⁴ gives similar results. We note that the energy for this experimentally based calculation jumps much greater spans of κ'/κ than occur in Fig. 17. Contributions to the net energy transfer at κ are distributed over a wide range of wavenumbers κ' . If the energy transfer were primarily local, $P(\kappa, \kappa')$ would be significantly different from zero only when κ'/κ is close to one. In Fig. 18, where the energy entering a wavenumber region (positive P) dominates that leaving (negative P), much of the energy entering comes from wavenumbers κ' that are about an order of magnitude lower than κ . On the other hand, when the dominant transfer is negative (not shown) much of the energy is passed on (jumps) to large κ' .²⁴

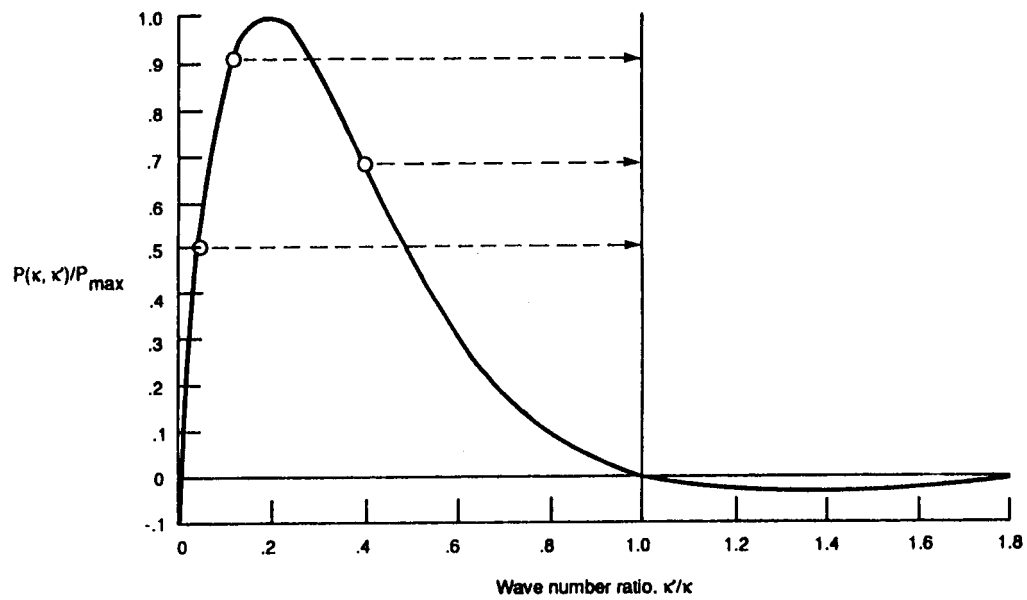


Figure 18. - Calculated contributions $P(\kappa, \kappa')$ to experimental energy transfer $T(\kappa)^{24}$ from wave numbers κ' . $\circ \rightarrow$ Energy transfers (jumps) from several κ' to κ , T , a maximum.

The tendency of the energy to jump between wavenumber regions that are separated appears to be in accord with the idea¹ that the turbulence tends to form concentrated regions of large velocity gradients. This tendency occurs even at low Reynolds numbers (see Fig. 5). Thus, when a low wavenumber eddy becomes unstable and forms a region of large velocity gradients, there will be a transfer of energy from a low to much higher wavenumbers.

It seems possible that the universal equilibrium theory¹ might apply in the presence of a rather high degree of nonlocalness of the spectral energy transfer, if the Reynolds number of the turbulence is very high. In that case, the energy spectrum extends over many decades of wavenumbers. Thus, there could be a cascade in which much of the energy is passed from low to high wavenumbers about a decade at a time. However the turbulence Reynolds number required to make the small eddies independent of the large ones would have to be larger than if the energy transfer were more local.

As a final note on nonlinear spectral transfer by turbulence self-interaction, we show that the production of small eddies by that mechanism can actually take place. We return to the unaveraged Navier-Stokes equations (Eqs. (1) and (2)), but omit the forcing term F_i , so that we have a decaying system. We again use Eqs. (3) and (4) for the initial conditions at $t = 0$. Those conditions are nonturbulent and have a single length scale. By solving Eqs. (1) and (2) numerically for several initial Reynolds

numbers,⁷ averaging $\overline{u_i u_i}$ over space to get $\overline{u_i u_i}$ as a function of time, and calculating the microscale λ from¹

$$\lambda^2 = - \nu \frac{\overline{u_i u_i}}{d\overline{u_i u_i}/dt}, \quad (30)$$

we obtain Fig. 19. The microscale is a measure of the size of the small eddies in the turbulence, and is defined by¹

$$\frac{\partial u_i}{\partial x_l} \frac{\partial u_i}{\partial x_l} \propto - \frac{\overline{u_i u_i}}{\lambda^2} \quad (31)$$

In Fig. 19 the microscale is normalized by its initial value and plotted against dimensionless time for several initial Reynolds numbers. Note that no closure assumption has been made in obtaining Fig. 19. As the Reynolds number increases, the small-scale structure becomes finer. The microscale decreases with increasing time until the fluctuation level (inertial effect) is low enough so that viscous forces prevent a further decrease. After λ decreases to a minimum it begins to grow. (Results for coarser and finer grids were not qualitatively different from these.) The increase of λ at later times is due to the selective annihilation of eddies by viscosity, the small eddies being the first to go. Thus, at large times, only the big eddies remain. It is this period of increasing λ , in which inertial (transfer) and viscous effects interact, that is generally observed experimentally in grid-generated turbulence (turbulence observed downstream of a grid

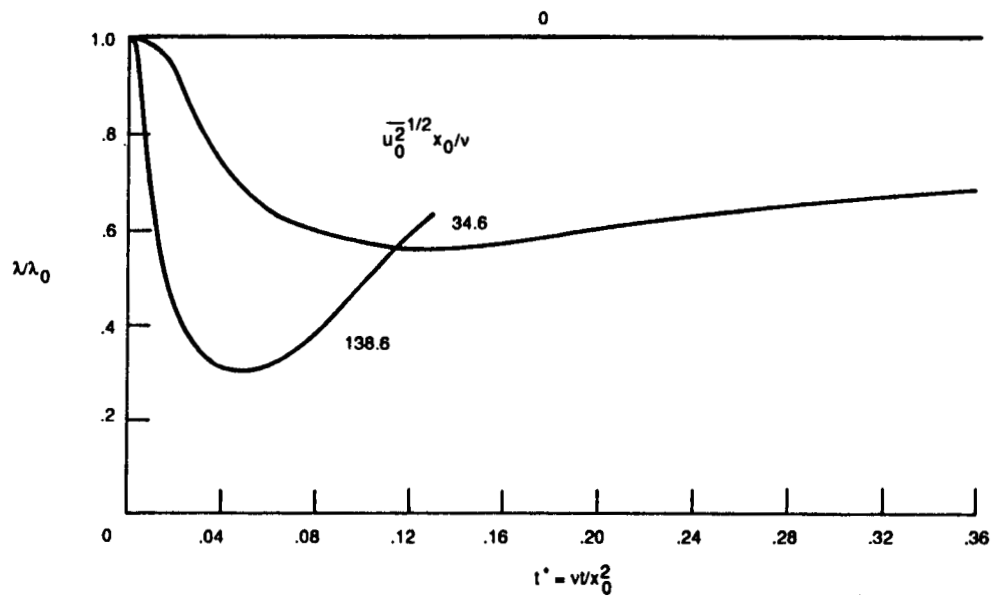


Figure 19. - Calculated evolution of microscale of velocity fluctuations (normalized by initial value) for various initial Reynolds numbers. No mean shear. Extrapolated to zero mesh size.

of wires or bars whose plane is normal to the flow in a wind tunnel). The increases of λ with time observed experimentally¹ are generally of the same order as those in Fig. 19 (doubling the time increases λ by a factor of about 1.5).

The early period, in which λ decreases with time, is of particular interest as illustrative of interwavenumber energy transfer. In order to generate the small-scale structure, turbulent energy must be transferred from big eddies to small ones.

Figure 20 shows the calculated evolution of mean-square velocity fluctuations $\overline{u^2} = \overline{u_1^2} = \overline{u_2^2} = \overline{u_3^2}$ for a series of initial Reynolds numbers. As the Reynolds number increases (v and initial length scale x_0 held constant), the rate of decay of $\overline{u^2}$ increases sharply, as in experimental turbulent flows.²⁶ This can be attributed to the nonlinear excitation of small-scale turbulent fluctuations at the higher Reynolds numbers. The high shear stresses between the small eddies cause a rapid decay.

B. Homogeneous turbulence with a mean shear

In order to study the nature of turbulence with shear, we again consider the simplest possible case. Considering the two-point moment equations for $\overline{u_i u_j}$ and for the pressure-velocity correlations,¹⁸ specializing those equations for homogeneous turbulence with a uniform shear, closing the system of equations by neglecting the triple-correlation terms, and taking their Fourier transforms, we get

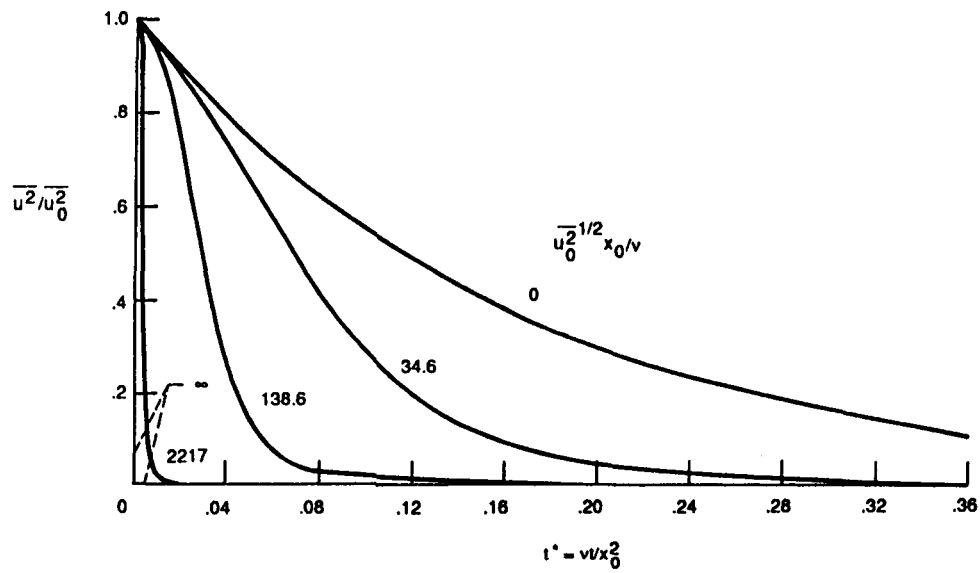


Figure 20. - Calculated evolution of microscale of velocity fluctuations (normalized by initial value) for various initial Reynolds numbers. No mean shear. $\overline{u^2} = \overline{u_1^2} = \overline{u_2^2} = \overline{u_3^2}$. Extrapolated to zero mesh size.

$$\begin{aligned} \frac{\partial}{\partial t} \varphi_{ij} = & -(\delta_{i1}\varphi_{2j} + \delta_{j1}\varphi_{i2}) \frac{dU_1}{dx_2} + \kappa_1 \frac{\partial \varphi_{ij}}{\partial \kappa_2} \frac{dU_1}{dx_2} \\ & + \left(2 \frac{\kappa_1 \kappa_j}{\kappa^2} \varphi_{2i} + 2 \frac{\kappa_1 \kappa_i}{\kappa^2} \varphi_{j2} \right) \frac{dU_1}{dx_2} - 2\nu \kappa^2 \varphi_{ij} . \end{aligned} \quad (32)$$

where φ_{ij} is the Fourier transform of $\overline{u_i u_j'}$ given by

$$\overline{u_i u_j'}(r) = \int_{-\infty}^{\infty} \varphi_{ij}(\kappa) e^{i\kappa \cdot r} d\kappa, \quad (33)$$

κ is the wavevector, r is the vector from point P to P' , u_i is a fluctuating velocity component, and dU_1/dx_2 is the mean velocity gradient in shear. Solution of Eq. (32) for initially isotropic turbulence gives, for φ_{ii} ,

$$\begin{aligned} \varphi_{ii} = & \frac{J_0 \{ \kappa_1^2 + [\kappa_2 + a\kappa_1(t - t_0)]^2 + \kappa_3^2 \}^2}{12\pi^2 \kappa^2} \\ & \cdot \exp \{ -2\nu(t - t_0)[\kappa^2 + a\kappa_1\kappa_2(t - t_0) + \frac{1}{3}a^2\kappa_1^2(t - t_0)^2] \} \\ & \cdot \left\{ \frac{\kappa^2}{\kappa_1^2 + [\kappa_2 + a\kappa_1(t - t_0)]^2 + \kappa_3^2} + 1 + \frac{\kappa_3^2 \kappa^2}{\kappa_1^2(\kappa_1^2 + \kappa_3^2)} \right. \\ & \cdot \left. \left[\tan^{-1} \frac{\kappa_2}{(\kappa_1^2 + \kappa_3^2)^{1/2}} - \tan^{-1} \frac{\kappa_2 + a\kappa_1(t - t_0)}{(\kappa_1^2 + \kappa_3^2)^{1/2}} \right]^2 \right\}, \end{aligned} \quad (34)$$

where $a = dU_1/dx_2$, and J_0 is a constant determined by the initial conditions. The spectral transfer term in Eq. (32) is, for φ_{ii} , $\kappa_1 \partial \varphi_{ii} / \partial \kappa_2 dU_1/dx_2$. If we integrate it over all directions in Fourier space to get T_{ii} , we obtain the dimensionless transfer

spectrum for shear plotted in Fig. 21. As required by Eq. (23), the net area under each curve is zero, so that T_{ij} gives zero contribution to the rate of change of $\overline{u_i u_i}$, it can only transfer energy from one part of wavenumber space to another.

The curves in Fig. 21 are predominately negative for small wavenumbers and positive for large ones, so that, in general, energy is transferred from small wavenumbers to large ones. Thus, the effect here is similar to that of the transfer term due to triple correlations in Fig. 16. The transfer affects the shape of the energy spectra (not shown) by exciting the higher wavenumber regions of those spectra, as is the case for the transfer due to triple correlations in Fig. 15.

A natural explanation of the transfer of energy to the high wavenumber regions by the mean velocity gradient would be that the velocity gradient stretches the vortex lines associated with the turbulence. This picture might also explain the small amount of reverse transfer shown in Fig. 21 for low wavenumbers at small velocity gradients, since the velocity gradient should be able to compress, as well as stretch, the vortex lines depending on how they are oriented. For large gradients the vortex lines would tend to all be oriented the same way, such that they are all stretched; in that case there is no reverse transfer. The reverse transfer at small shear might explain why experiments sometimes show turbulence scales larger than those associated with the turbulence generators.²⁷

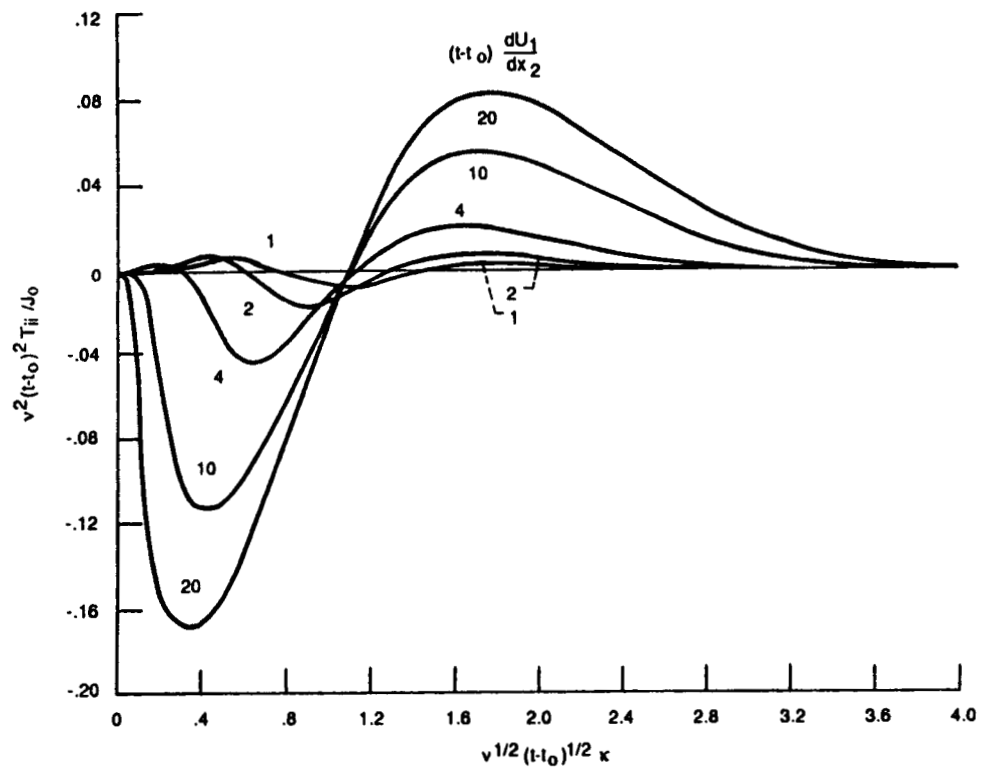


Figure 21. - Dimensionless spectra of transfer term due to mean velocity gradient in Equation (32).

An alternative explanation of the energy transfer between wavenumbers would be that the large eddies break up into smaller ones. That mechanism seems to give a natural explanation for the suddenness of turbulent mixing considered in section V, but may not easily explain the reverse transfer observed in Fig. 21. Of course, there is no reason why the stretching or compressing of vortex lines could not be sudden.

As in the last section, we consider turbulent solutions of the unaveraged Navier-Stokes equations in attempting to show the actual effect on turbulence of certain processes. Here we again solve numerically Eqs. (1) and (2) without the forcing term, but this time we impose a uniform mean shear on the turbulence.

In Figs. 22 and 23 we show the effect on homogeneous turbulence of suddenly removing the mean shear. Figure 22 shows that the shear produces considerable anisotropy, although it was initially isotropic at $t = 0$. Upon removal of the mean shear the turbulence quickly returns to isotropy. That is, the three components of $\overline{u_i^2}$ quickly equalize. The pressure-velocity-gradient correlations in Eq. (18) are thus successful in transferring energy among the various directional components in such a way that equality of the $\overline{u_i^2}$ is produced (see also the equivalent term in Eq. (32), the last term proportional to dU_1/dx_2). We note that $\overline{u_2^2}$ continues to increase for a short time after the shear is removed, probably because it receives

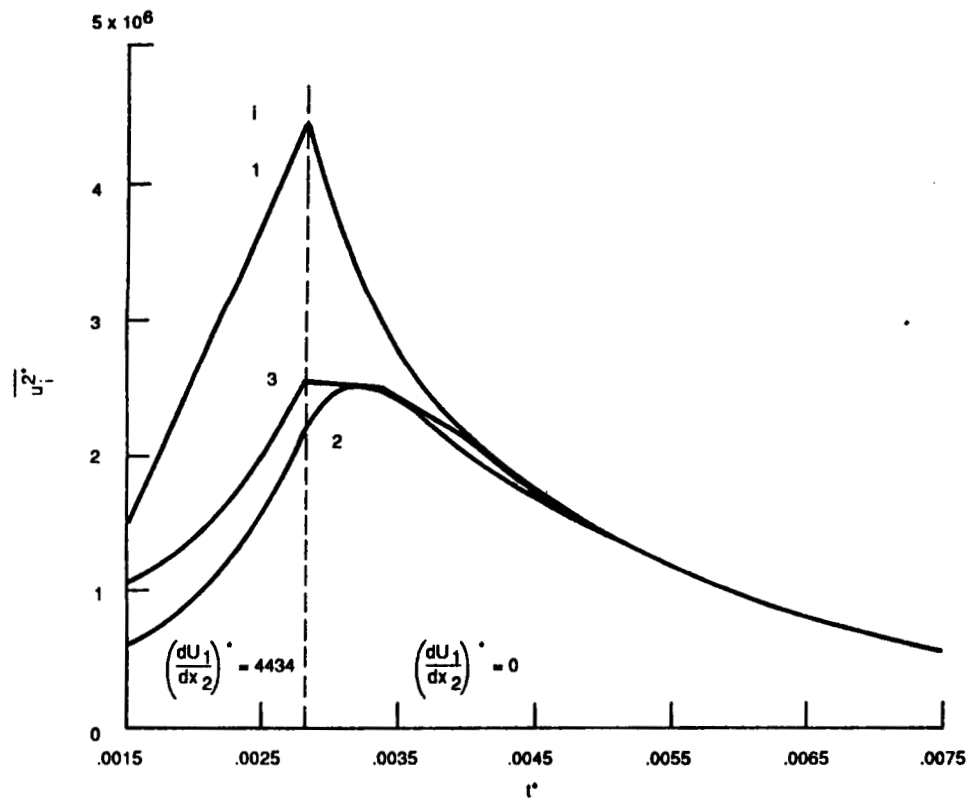


Figure 22. - Calculated approach to isotropy of uniformly sheared turbulence, upon sudden removal of the shear. $\overline{u_0^2}^{1/2} x_0 / \nu = 1108$. 32^3 grid points. Starred quantities nondimensionalized by x_0 and ν .

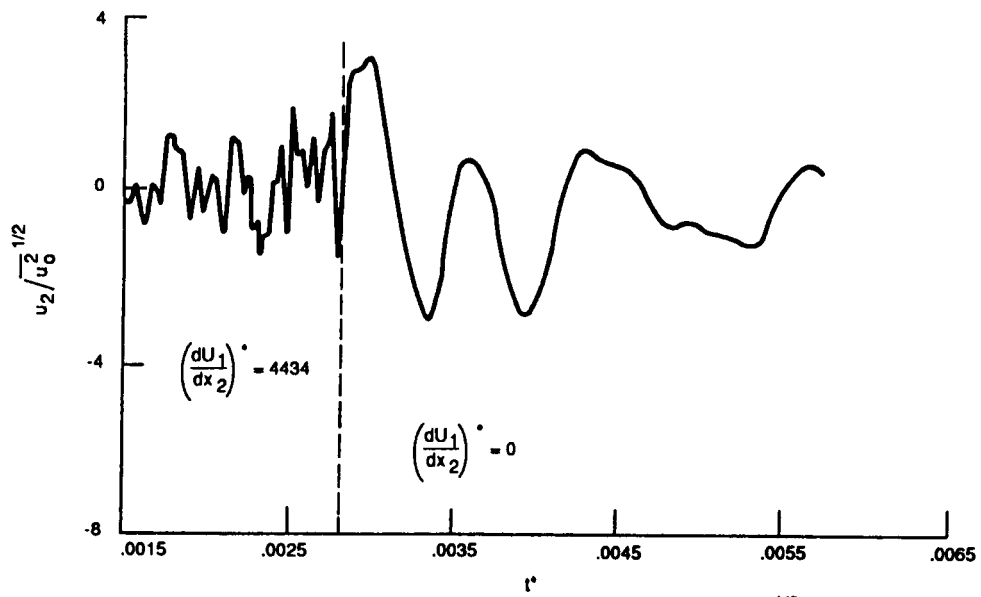


Figure 23. - Effect of removal of uniform shear on structure of turbulence. $\overline{u_0^2}^{1/2} x_0 / \nu = 1108.32^3$ grid points. Starred quantities nondimensionalized by x_0 and ν .

energy from both $\overline{u_1^2}$ and $\overline{u_3^2}$. In addition to equalization of the three directional components of $\overline{u_i^2}$, removal of the mean shear is found to destroy the turbulent shear stress $-\rho\overline{u_1u_2}$.

Figure 23 gives a comparison of the evolution of u_2 before and after removal of the mean shear. The mean shear produces a small-scale structure in the turbulence which disappears almost immediately when dU_1/dx_2 goes to zero, evidently because of the large fluctuating shear stresses between the small-scale eddies.

Figure 23 shows, in a particularly graphic manner, the effectiveness of the mean-gradient transfer term $\kappa_1\partial\phi_{ij}/\partial\kappa_2 dU_1/dx_2$ in Eq. (32) in producing small-scale turbulent structure. We first showed the existence of, and calculated, a mean-gradient transfer term almost three decades ago.¹⁸ The results shown here⁷ are a graphic demonstration of the effectiveness of that term in producing a small-scale structure in turbulence.

V. THE SUDDENNESS OF TURBULENT MIXING

A fundamental question about the nature of turbulence concerns how turbulent mixing takes place. Here we consider the *instantaneous* turbulent mixing which occurs in the presence of mean velocity and/or temperature gradients.

Consider first the effect of turbulence on the shear stress and/or heat transfer. To do that, split the velocity and pressure in Eq. (1) into mean and fluctuating components (Reynolds decomposition) and take average values. This gives, for $F_i = 0$,⁷

$$\rho \frac{\partial U_i}{\partial t} = - \rho U_k \frac{\partial U_i}{\partial x_k} - \frac{\partial P}{\partial x_i} + \frac{\partial}{\partial x_k} \left[\rho \nu \frac{\partial U_i}{\partial x_k} - \rho \overline{u_i u_k} \right] \quad (35)$$

where U_i and P are mean quantities and the u_i are now fluctuating components ($\overline{u_i} = 0$). (In Eq. (1) the u_i represented mean plus fluctuating components.) Equation (35) has the same form as Eq. (1), but the viscous stress $\rho \nu \partial U_i / \partial x_k$ is augmented by the term $-\rho \overline{u_i u_k}$, where the overbar designates an averaged value. Thus $-\rho \overline{u_i u_k}$ increases the effective stress and is called the turbulent or Reynolds stress. A similar operation on the unaveraged energy equation shows that turbulence augments the heat transfer by the term $-\rho C \overline{\tau u_k}$, where τ is the turbulent temperature fluctuation ($\overline{\tau} = 0$), and C is the specific heat. These observations apply whether the turbulence is homogeneous or inhomogeneous.

We note that the expression for the turbulent stress corresponds exactly with that for the molecular stress obtained in

the kinetic theory of gases.²⁸ It is only necessary to replace the macroscopic velocities in $-\rho \overline{u_i u_k}$ by molecular velocities. A similar correspondence exists in the expressions for the turbulent and molecular heat transfer.

Let us see what the presence of the turbulent stress and heat transfer terms in the equations for mean flow and heat transfer implies about the instantaneous turbulent mixing. Instantaneous mixing refers here to the mixing one would see in a snapshot taken at a particular time.

Note first what would happen if the spatial pattern of instantaneous turbulent mixing were uniform, or nearly so. If that were the case, a portion of fluid as it moves transversely in mean velocity and temperature gradients (mean velocity in the x_1 -direction) would have a uniform tendency (because of uniform mixing) to assume the mean x_1 -momentum and temperature of the surrounding fluid at each point along its path. That tendency would increase with increasing turbulence intensity or Reynolds number, because small-scale motions become excited with increasing turbulence intensity (see Section IV), and so the turbulent mixing (average or instantaneous) increases. (Note that turbulent mixing takes place most efficiently by small-scale motions, since those provide the most intimate contact of the fluid entering a region with that already there.)

Thus if the instantaneous turbulent mixing were spatially uniform, the tendency of a portion of fluid to assume the mean

x_1 -momentum and temperature of the surrounding fluid at each point as it moves transversely would increase with increasing turbulence intensity. That would, however, cause the fluctuations from the mean, u_1 and τ in the turbulent stress $\overline{\rho u_i u_j}$ and heat transfer $\overline{\rho C \tau u_j}$ to decrease in magnitude with increasing turbulence intensity or Reynolds number. The stress component $\overline{\rho u_1^2}$ would then decrease. But that trend is unphysical and does not occur. In fact, as might be expected, the opposite trend occurs; as turbulence intensity $(\overline{u_i u_i}/3)^{1/2}$ or Reynolds number increases, $\overline{u_1^2}$ increases.²⁹

The instantaneous turbulent mixing therefore cannot be spatially uniform, or nearly so, as assumed in obtaining the above unphysical trend. There must be regions of relative quiescence if x_1 -momentum and heat are to be transferred turbulently at high turbulence intensities. But in that case there must also be regions where the instantaneous mixing is relatively intense and localized, since that is the only way the average mixing could be high for high turbulence intensities, when regions of quiescence are present. So the only sensible assumption about the instantaneous mixing is that it is small except in localized regions, where it is intense. Then the above unphysical trends do not occur, since the tendency of a portion of fluid, as it travels transversely, to assume the mean x_1 -momentum and temperature of the surrounding fluid is sudden and is confined to localized regions. This is particularly true for high turbulence intensities or Reynolds

numbers. There the fluctuations from the mean can be large for most times and spatial positions. Thus, although fluid turbulence occurs in a continuum, changes in the momentum and temperature of a moving portion of fluid tend to be sudden and localized.

Our observation here concerning the suddenness of turbulent mixing seems to be congruous with what we said in section IV about the transfer of energy between wavenumber bands that are widely separated. Thus, if an eddy suddenly mixes with the surrounding fluid, as was found to occur in the present section, that would most likely, for efficient mixing, take place by a sudden breakup or shattering of the large eddy into many smaller ones at the point of mixing, with a consequent transfer of energy from a small wavenumber band to much larger ones. As mentioned earlier, turbulent mixing takes place most efficiently by small-scale motions, since those provide the most intimate contact of the fluid entering a region with that already there. Thus, the transfer of energy associated with the presence of mean gradients, like that due to turbulence self-interaction, tends to take place between wavenumber bands that are considerably separated.

The localness or suddenness of the turbulent transfer considered in this section also seems to be in agreement with the concept of bursting coherent structures in shear flow near a wall. Much work has recently been done on that phenomenon.³⁰

Although our purpose here is to consider the nature of turbulent mixing, rather than to lend credence to any particular

expressions for the turbulent shear stress or heat transfer, it is of interest that our present result is in agreement with an assumption of Prandtl's mixing-length theory.³¹ According to the mixing-length hypothesis a certain suddenness in the turbulent mixing must occur for turbulent transfer to take place. The mixing length expressions for $\overline{u_1 u_2}$ and $\overline{\tau u_2}$ are

$$\overline{u_1 u_2} = - \overline{u_2} \ell_2 \frac{dU_1}{dx_2} \quad (36)$$

and

$$\overline{\tau u_2} = - \overline{u_2} \ell_2 \frac{dT}{dx_2} , \quad (37)$$

where T is the mean temperature and ℓ_2 is an effective transverse distance a portion of fluid moves before mixing with the fluid. Thus, if the mixing took place continuously, ℓ_2 would be zero, and the turbulent shear stress and heat transfer would be zero.

This leads us to a comparison between mixing-length theory and the elementary kinetic theory of molecular transport. The mixing-length expressions given by Eqs. (36) and (37) are, in fact very similar to those obtained in the elementary kinetic theory.³² It is only necessary to identify the macroscopic velocities, temperatures, and lengths in the barred quantities in Eqs. (36) and (37) with molecular quantities in kinetic theory (e.g., with molecular velocities and free paths). It is of interest that it was apparently kinetic theory that originally inspired turbulent mixing-length theory; the mixing length was supposed by Prandtl to

be something like the mean-free path in kinetic theory.³¹ The transfer mechanisms for the two types of systems appear to be similar. As shown in this section, turbulent transfer, like encounters between particles, tends to be somewhat sudden. This similarity occurs in spite of the fact that turbulent systems are continuous and dissipative, whereas particle systems are discrete and conservative. However, particle systems are like turbulent systems in that they are nonlinear and display sensitive dependence on initial conditions.³³

VI. CONCLUSION

Navier-Stokes turbulence is a chaotic phenomenon. Our long-term solutions with steady forcing show that the calculated turbulence has a positive Liapunov exponent, which in turn means that it is sensitively dependent on initial conditions.

Turbulence has, for a long time, been assumed to be random,¹ or at least to have the appearance of randomness. Sensitive dependence on initial conditions provides an explanation for the occurrence of apparent randomness in turbulence. But in spite of its random appearance turbulence has a deterministic element, in as much as the Navier-Stokes equations which describe it are fully deterministic. The phrase "deterministic chaos" might therefore provide a fitting description for turbulence. Although turbulence is time-dependent and random in appearance, our solutions show that it can form with no time-dependent or random input. This again is a result of sensitive dependence of the solutions on initial conditions.

It may not, however, be a sufficiently complete description of turbulence to say that it is chaotic. Some of our low-Reynolds-number flows have a positive Liapunov exponent, and thus are chaotic, but their Poincaré sections show a pattern in some of their parts. On the other hand, solutions at somewhat higher Reynolds numbers show a complete lack of pattern. Perhaps we should reserve the

term "turbulent" for flows that have a positive Liapunov exponent and, in addition, have Poincaré sections without pattern.

Turbulence is also aperiodic or nonperiodic. As examples of flows which contrast with turbulence, we were able to obtain some periodic and fixed-point solutions. Whereas the fixed-point (in phase space) flows are time-independent, and the periodic flows are closed lines in phase space (points on Poincaré sections), the turbulent flows are time-dependent and fill a portion of phase space. The turbulent, periodic, and fixed-point flows are all attracted to lower dimensional regions of phase space called attractors. The turbulent flows lie on strange or chaotic attractors.

Another requirement that is often given for flows to be turbulent is that they have negative velocity-derivative skewness factors. However, our periodic and fixed-point solutions have skewness factors that do not vary greatly from those for turbulent flows. A negative skewness factor seems to be more an indication of nonlinearity (all of our forced flows are highly nonlinear) than of turbulence.

By using the instantaneous Navier-Stokes equations for decaying turbulence, as well as their corresponding moment equations, it is shown that the energy in turbulence moves between wavenumber bands, primarily from low wavenumbers to higher ones. That can occur for both homogeneous and inhomogeneous turbulence. The energy transfer can take place as a result of nonlinear

self-interaction as well as of interaction between turbulence and mean gradients. In both cases the transfer takes place primarily between wavenumbers that are considerably separated, rather than between neighboring wavenumbers; the energy often jumps between wavenumbers differing by about an order of magnitude. Closely related to these energy jumps is the observation that turbulent mixing in the presence of mean gradients takes place in localized regions where eddies shatter, separated by relatively quiescent regions.

There is an interaction between spectral energy transfer and dissipation. The former excites the high wavenumber regions of the spectrum by transferring energy into them. That, in turn, increases the dissipation because of the high shear stresses between the small-scale components.

Also, energy transfer among directional components is produced by the pressure term in the Navier-Stokes equations. That causes a return to isotropy of turbulence which was initially isotropic, but which had become anisotropic in the presence of mean shear.

Navier-Stokes turbulence and kinetic-theory systems are compared. In spite of the fact that the two types of systems are fundamentally different, the former being continuous and dissipative, the latter being discrete and conservative particle systems, there are essential similarities. Both types of systems are nonlinear and display sensitive dependence on initial

conditions, and so are chaotic. As a result of their chaoticity, both have a random appearance. Moreover, turbulent mixing in a continuous fluid and encounters between discrete particles are similar in that both show a certain suddenness or localness. However there does not seem to be anything in simple particle systems which is comparable to the energy cascades to small scales of motion which occur in turbulence.

REFERENCES

- ¹G.K. Batchelor, The Theory of Homogeneous Turbulence, (Cambridge University Press, New York, 1953).
- ²J.R. Herring, "An Introduction and Overview of Various Theoretical Approaches to Turbulence," in Theoretical Approaches to Turbulence, edited by D.L. Dwyer, M.Y. Hussaini, and R.G. Voigt. (Springer-Verlag, New York, 1985), pp. 73-90.
- ³R.H. Kraichnan, "Decimated Amplitude Equations in Turbulence Dynamics," in Theoretical Approaches to Turbulence, edited by D.L. Dwyer, M.Y. Hussaini, and R.G. Voigt (Springer-Verlag, New York, 1985), pp. 91-136.
- ⁴R.G. Deissler, "Turbulence Processes and Simple Closure Schemes," in Handbook of Turbulence, edited by W. Frost and T.H. Moulden (Plenum Press, New York, 1977), vol. I, pp. 165-186.
- ⁵D. Ruelle, and F. Takens, "On the Nature of Turbulence," *Commun. Math. Phys.* 20(3), 167-192 (1971).
- ⁶A.J. Lichtenberg and M.A. Lieberman, Regular and Stochastic Motion, (Springer-Verlag, New York, 1983).
- ⁷R.G. Deissler, "Turbulent Solutions of the Equations of Fluid Motion," *Rev. Mod. Phys.* 56, 223-254 (1984). Recent calculations in which a pseudospectral rather than a finite-difference method was used, and in which the number of numerical grid points was increased from 32^3 to 128^3 , also show that decaying turbulence (no mean gradients) exhibits sensitive dependence on initial conditions.
- ⁸R.G. Deissler, "Is Navier-Stokes Turbulence Chaotic?" *Phys. Fluids* 29, 1453-1457 (1986).
- ⁹R.J. Deissler, "External Noise and the Origin and Dynamics of Structure in Convectively Unstable Systems," *J. Stat. Phys.* 54(5/6), 1459-1488 (1989).
- ¹⁰P. Constantin, C. Foias, O.P. Manley, and R. Temam, "Determining Modes and Fractal Dimension of Turbulent Flows," *J. Fluid Mech.* 150, 427-440 (1985).
- ¹¹R.A. Clark, J.H. Ferziger, and W.C. Reynolds, "Evaluation of Subgrid-Scale Models Using an Accurately Simulated Turbulent Flow," *J. Fluid Mech.* 91, 1-16 (1979).

- ¹²S. Tavoularis, S. Corrsin, and J.C. Bennett, "Velocity-Derivative Skewness in Small Reynolds Number, Nearly Isotropic Turbulence," J. Fluid Mech. 88, 63-69 (1978).
- ¹³P. Constantin, C. Foias, and R. Teman, Attractors Representing Turbulent Flows, Memoirs, Amer. Math. Soc. 53 (314), 1985, p. 57.
- ¹⁴H. Haken, Advanced Synergetics (Springer, New York, 1983).
- ¹⁵J.D. Farmer, E. Ott, and J.A. Yorke, "The Dimension of Chaotic Attractors," Physica 7D, 153-180 (1983).
- ¹⁶J. Guckenheimer and G. Buzyna, "Dimension Measurements for Geostrophic Turbulence," Phys. Rev. Lett. 51 (16), 1438-1441 (1983).
- ¹⁷R. G. Deissler, "Spectral Energy Transfer for Inhomogeneous Turbulence," Phys. Fluids 24 (10), 1911-1912 (1981).
- ¹⁸R.G. Deissler, "Effects of Inhomogeneity and of Shear Flow in Weak Turbulent Fields," Phys. Fluids 4 (10), 1187-1198 (1961).
- ¹⁹A. Craya, "Contribution a l'Analyse de la Turbulence Associee a des Vitesses Moyennes," Publ. Sci. Tech. Minist. Air Fr. 345, (1958).
- ²⁰R.G. Deissler, "On the Decay of Homogeneous Turbulence Before the Final Period," Phys. Fluids 1 (2), 111-121 (1958).
- ²¹R. G. Deissler, "Comparison of a Correlation Term-Discard Closure for Decaying Homogeneous Turbulence With Experiment," Phys. Fluids 22 (1), 185-186 (1979).
- ²²R.G. Deissler, "A Theory of Decaying Homogeneous Turbulence," Phys. Fluids 3 (2), 176-187 (1960).
- ²³W.L. Miller and A.R. Gordon, "Numerical Evaluation of Infinite Series and Integrals Which Arise in Certain Problems of Linear Heat Flow, Electrochemical Diffusion, etc.," J. Phys. Chem. 35, 2785-2884 (1931).
- ²⁴R.G. Deissler, "On the Localness of the Spectral Energy Transfer in Turbulence," Appl. Sci. Res. 34, 379-392 (1978).
- ²⁵S.C. Ling and T.T. Huang, "Decay of Weak Turbulence," Phys. Fluids 13 (12), 2912-2924 (1970).

- ²⁶R.G. Deissler, "Decay of Homogeneous Turbulence From a Given State at Higher Reynolds Number," *Phys. Fluids* 22 (10), 1852-1856 (1979).
- ²⁷R.G. Deissler, "Comparison of Theory and Experiment for Homogeneous Turbulence With Shear," *Phys. Fluids* 18 (10), 1237-1240 (1975).
- ²⁸B.S. Tanenbaum, Plasma Physics, (McGraw-Hill, 1967), pp. 162-164.
- ²⁹J. Laufer, The Structure of Turbulence in Fully Developed Pipe Flow, NACA Rept. 1174 (1954).
- ³⁰A.K.M.F. Hussain, "Coherent Structures-Reality and Myth," *Phys. Fluids* 26 (10), 2816-2850 (1983).
- ³¹B.A. Bakhmeteff, The Mechanics of Turbulent Flow, (Princeton University Press, Princeton, NJ, 1936).
- ³²S. Chapman and T.G. Cowling, The Mathematical Theory of Non-Uniform Gases, 2nd ed. (Cambridge University Press, New York, 1953).
- ³³S.D. Stoddard and J. Ford, "Numerical Experiments on the Stochastic Behavior of a Lennard-Jones Gas System," *Phys. Rev. A* 8 (3), 1504-1512 (1973).

Report Documentation Page

1. Report No. NASA TM-101983		2. Government Accession No.		3. Recipient's Catalog No.	
4. Title and Subtitle On the Nature of Navier-Stokes Turbulence				5. Report Date May 1989	
				6. Performing Organization Code	
7. Author(s) Robert G. Deissler				8. Performing Organization Report No. E-4682	
				10. Work Unit No. 505-90-01	
9. Performing Organization Name and Address National Aeronautics and Space Administration Lewis Research Center Cleveland, Ohio 44135-3191				11. Contract or Grant No.	
				13. Type of Report and Period Covered Technical Memorandum	
12. Sponsoring Agency Name and Address National Aeronautics and Space Administration Washington, D.C. 20546-0001				14. Sponsoring Agency Code	
15. Supplementary Notes This report was a dissertation submitted in partial fulfillment of the requirements for the Degree of Doctor of Philosophy to the Department of Mechanical and Aerospace Engineering, Case Western Reserve University, Cleveland, Ohio in May 1989.					
16. Abstract Several turbulent and nonturbulent solutions of the Navier-Stokes equations are obtained. The unaveraged equations are used numerically in conjunction with tools and concepts from nonlinear dynamics, including time series, phase portraits, Poincaré sections, largest Liapunov exponents, power spectra, and strange attractors. Initially neighboring solutions for a low-Reynolds-number fully developed turbulence are compared. The turbulence is sustained by a nonrandom time-independent external force. The solutions, on the average, separate exponentially with time, having a positive Liapunov exponent. Thus the turbulence is characterized as chaotic. In a search for solutions which contrast with the turbulent ones, the Reynolds number (or strength of the forcing) is reduced. Several qualitatively different flows are noted. These are, respectively, fully chaotic, complex periodic, weakly chaotic, simple periodic, and fixed-point. Of these, we classify only the fully chaotic flows as turbulent. Those flows have both a positive Liapunov exponent and Poincaré sections without pattern. By contrast, the weakly chaotic flows, although having positive Liapunov exponents, have some pattern in their Poincaré sections. The fixed-point and periodic flows are nonturbulent, since turbulence, as generally understood, is both time-dependent and aperiodic. By using both the unaveraged Navier-Stokes equations, and the corresponding averaged or moment equations, turbulent solutions are obtained in which energy cascades from large to small-scale motions. In general, the spectral energy transfer takes place between wavenumber bands that are considerably separated. The spectral transfer can occur either as a result of nonlinear turbulence self-interaction or by interaction of turbulence with mean gradients. The latter appears to be closely related to a nonuniform or sudden turbulent mixing shown to occur in the presence of mean gradients. Turbulent systems are compared with those studied in kinetic theory. The two types of systems are fundamentally different (continuous and dissipative as opposed to discrete and conservative), but there are similarities. For instance, both are nonlinear and show sensitive dependence on initial conditions. Also, the turbulent and molecular stress tensors are identical if the macroscopic velocities for the turbulent stress are replaced by molecular velocities.					
17. Key Words (Suggested by Author(s)) Turbulence; Chaos; Navier-Stokes; Nonlinear; Liapunov exponent; Phase portrait; Energy transfer; Poincaré sections			18. Distribution Statement Unclassified - Unlimited Subject Category 34		
19. Security Classif. (of this report) Unclassified		20. Security Classif. (of this page) Unclassified		21. No of pages 102	
				22. Price* A06	